Microstructure and dimensional stability of slag-based high-workability concrete with steelmaking slag aggregate and fibers

Vanesa Ortega-López [1], Víctor Revilla-Cuesta [2] *, Amaia Santamaría [3], Aimar Orbe [4], Marta Skaf [5]

[1] Position: Associate Professor
Department of Civil Engineering, Escuela Politécnica Superior, University of Burgos, c/ Villadiego s/n, 09001 Burgos, Spain.
Email: vortega@ubu.es

[2] Position: Postdoctoral Research Associate
Department of Civil Engineering, Escuela Politécnica Superior, University of Burgos, c/ Villadiego s/n, 09001 Burgos, Spain.
Email: vrevilla@ubu.es

[3] Position: Assistant Professor
Department of Mechanical Engineering, Escuela de Ingeniería de Bilbao I (bloque B), University of the Basque Country, Pl. Ingeniero Torres Quevedo 1, 48013 Bilbao, Spain.
Email: amaia.santamaria@ehu.es

[4] Position: Associate Professor
Department of Mechanical Engineering, Escuela de Ingeniería de Bilbao I (bloque B), University of the Basque Country, Pl. Ingeniero Torres Quevedo 1, 48013 Bilbao, Spain.
Email: aimar.orbe@ehu.es

[5] Position: Associate Professor
Department of Construction, Escuela Politécnica Superior, University of Burgos, c/ Villadiego s/n, 09001 Burgos, Spain.
Email: mskaf@ubu.es

***Corresponding Author**:
Víctor Revilla-Cuesta
Department of Civil Engineering, University of Burgos.
Escuela Politécnica Superior. Calle Villadiego s/n, 09001 Burgos, Spain.
Phone: +34947497117
e-mail: vrevilla@ubu.es

Abstract

Four high-workability (pumpable and self-compacting) concrete mix designs are presented that incorporate steelmaking slags with additions of both metallic and polymeric fibers. Electric Arc Furnace Slag (EAFS) as aggregate, and Ladle Furnace Slag (LFS) and Ground Granulated Blast Furnace Slag (GGBFS) as Supplementary Cementitious Material (SCM) are applied to optimize the sustainability of the mix design. The main variables in the microstructural analysis, the porosity and the pore structure of the hardened mixes, were assessed with Mercury Intrusion Porosimetry (MIP), X-ray Computed Tomography (XCT) and water capillary penetration analysis. Moreover, shrinkage was observed to decrease when adding metallic fibers and LFS. In general, Scanning Electron Microscopy (SEM) observations revealed good quality concrete microstructures. Accelerated aging tests at a moderate temperature (72°C) produced a slight lengthening, which affected the dimensional stability of all the mixtures, which was also conditioned by their micro-porosity. The internal damage induced by this test decreased the brittle fracture strength of the concrete mixes, although the use of GGBFS and LFS moderated that damage, due to the increased compliance of the cementitious matrix.

Keywords: electric arc furnace slag; ground granulated blast furnace slag; ladle furnace slag; fiber-reinforced high-workability concrete; concrete microstructure and porosity; dimensional stability.

Acronyms: Ground Granulated Blast Furnace Slag (GGBFS); Electric Arc Furnace Slag (EAFS); Interfacial Transition Zones (ITZ); Ladle Furnace Slag (LFS); Mercury Intrusion Porosimetry (MIP); Scanning Electron Microscopy (SEM); Supplementary Cementitious Materials (SCM); Ultrasonic Pulse Velocity (UPV); water-to-binder ratio (w/b); water-to-cement ratio (w/c); X-ray Computed Tomography (XCT).

1. Introduction

In 1984, the United Nations published the *"Brundtland Report"* with the title "*Our Common Future*". This report defined the concept of sustainable development as "development that meets the needs of the present without compromising the ability of future generations to meet their own needs" (Hák et al. 2018). Balancing economic, environmental and social dimensions can contribute to the achievement of this goal (Revilla-Cuesta et al. 2020b), grounded in sustainable development education for younger generations, and through improvements to the sustainability of various productive sectors (Martínez-Lage et al. 2020; San-José and Manso 2006). Among them, the construction sector must be exemplary in the adoption of measures that will significantly increase its sustainability, due to its high environmental impacts (Bahramian and Yetilmezsoy 2020) such as waste generation (Silva et al. 2019) and CO_2 emission levels (Dong et al. 2020). Using industrial wastes and by-products to manufacture materials such as concrete (Revilla-Cuesta et al. 2020a) and asphalt mixes (Skaf et al. 2019) is one of the most widespread and accepted measures of sustainability in this sector. This paper is focused on iron and steelmaking slags, materials that can be used very successfully to enhance the sustainability of hydraulic concrete, due to their good performance (Branca et al. 2020). The usefulness of reusing this industrial by-product in cement-based mixes is clear, as approximately 50 Mt of slag are produced in the European Union alone per year and often deposited in landfills .

Various types of slag, used either as aggregates or as binders, have shown good behavior in concrete (Fronek et al. 2012; Yildirim and Prezzi 2020). A sustainable concrete can contain either:

- Electric Arc Furnace Slag (EAFS) stands out among the different types of slag that can be used as aggregate (Bosela et al. 2009; Ladomerský et al. 2016). EAFS is obtained during the process of manufacturing steel from ferrous scrap in an electric furnace (Abu-Eishah et al. 2012). It is a gravelling product mainly characterized by its high density (Roslan et al. 2020) and good mechanical performance (Fuente-Alonso et al. 2017), yielding optimal quality Interfacial Transition Zones (ITZ) with the cementitious matrices (Brand and Roesler 2018). However, careful design of the concrete mix that incorporates this sort of waste is important (Santamaría et al. 2017), especially in relation to the fine aggregate fraction, as the superficial roughness of EAFS, as well as its high density, generally hinders adequate in-fresh workability (Qasrawi 2018).
- Ground Granulated Blast Furnace Slag (GGBFS) is obtained after abrupt cooling and subsequent milling of Blast Furnace Slag, while Ladle Furnace Slag (LFS) is a dusty material that forms after slow cooling of slag produced during the steel refining process (Sideris et al. 2018). Both have been used over various decades for soil stabilization (Manso et al. 2013) and cement production (Parron-Rubio et al. 2018). However, their use as Supplementary Cementitious Materials (SCM) in concrete production has only been demonstrated over recent years (Bondar et al. 2019). In comparison with conventional clinker, GGBFS is lighter (Mehta et al. 2020), needs higher grinding fineness (Zhang et al. 2020) and its strength development is slower (Majhi and Nayak 2020). The main characteristic of LFS is its expansiveness, although this type of slag is also lighter and slowly develops its strength (Ortega-López et al. 2014).

While the mechanical properties of concretes made with these by-products have been evaluated in the literature, there are two related aspects that have yet to be studied in detail: concrete porosity and its dimensional stability. These two properties are also closely related to concrete strength (Arriagada et al. 2019) and durability (Zhan and He 2019), so their study is essential to analyze the validity of these sorts of sustainable concretes in real structures (Zanini 2019).

- The analysis of concrete porosity has, in recent years, gained greater importance as an aspect of importance, due to the development of such techniques as X-ray Computed Tomography (XCT) (Koenig 2020). Its precise evaluation is necessary, because higher porosity levels imply lower strength and deeper penetration levels of external damaging agents within the concrete (Ortega-López et al. 2018).
- The alteration of the dimensions of the concrete (phenomena of dimensional instability, such as shrinkage or lengthening) can locally cause tensile and compressive stresses, which can lead to the

appearance of macro- or micro-cracks (Yang et al. 2019). Those cracks have negative effects on both the strength and the durability performance of the concrete (Li et al. 2016). Its dimensional stability is conditioned by the mix composition and, therefore, by the addition of slag or fibers. On the one hand, it is known that long-term shrinkage slightly increases in concretes containing EAFS rather than natural aggregates (Lee et al. 2019). Furthermore, LFS in contact with moisture and CO_2 can show long-term expansive properties that could lead to cracking problems (Lim et al. 2019); however, this expansiveness of LFS could be useful to counteract concrete shrinkage (Papayianni et al. 2018). A precise quantity of LFS must therefore be defined to add to the concrete mix to achieve an adequate balance between both aspects (Santamaria et al. 2018). On the other hand, the addition of fibers is known to improve strength against brittle fracture (Liew and Akbar 2020). This performance is due to fibers which sew the cracks (bridging effect) and improve the residual strength of the concrete after cracking and failure (Larsen and Thorstensen 2020). Furthermore, their effect is beneficial for shrinkage, because the fibers act as rigid elements that counteract any shortening or lengthening of the concrete (Afroughsabet et al. 2016) but, in general, its use is considered as negative with regard to sustainability.

Both dimensional variations and porosity must be studied in good-quality structural concrete, using high-workability mixtures tested in the fresh state and showing good strengths at 28 days (close to 50 MPa). It is clear that any excess water, *i.e.*, water neither adsorbed nor absorbed by the mix components, but needed to reach high fluidity, will evaporate after the mixing process, increasing both porosity and short-term plastic shrinkage (Revilla-Cuesta et al. 2020a). Furthermore, additions of EAFS, fibers and slag-based binders can significantly change both the porosity and the dimensional stability of concrete. Hence, the challenge to design reliable mixtures that meet the basic in-fresh conditions and optimize the resultant properties is hardly trivial.

This knowledge gap is addressed in this study through the analysis of four high-workability concrete mix designs made with large amounts of EAFS, GGBFS and/or LFS, as well as either metallic or polymeric fibers. The mixtures were analyzed to determine their porosity (Mercury Intrusion Porosimetry, MIP; X-ray Computed Tomography, XCT; and capillary water absorption tests) and to determine their dimensional stability (setting shrinkage, long-term shrinkage and accelerated aging tests to assess eventual expansive behavior). This paper is included in a set of four articles (Ortega-López et al. 2021; Santamaría et al. 2021; Santamaría et al. 2020b) dealing with this kind of concrete mixes.

2. Materials and methods

The properties of the materials and the experimental plan of this study are discussed in this section.

2.1. Cement, water, admixture and LFS

Regarding the hydraulic binder, on the one hand, two different cements were used: CEM III/B 32.5 N and CEM II/B-S 42.5 N as per EN 197-1 (EN-Euronorm), with around 70 % and 30 % GGBFS, respectively. On the other hand, the effect of the joint use of 6 % LFS as a Supplementary Cementitious Material (SCM) with CEM III/B 32.5 N was also studied. The LFS had a loss on ignition of 0.5 % and a specific weight of 3.03 Mg/m^3. Its chemical composition and X-Ray Diffraction (XRD) analyses are presented in Table 1 and its gradation is plotted in Figure 1 (fineness modulus of 0.75 units).

An admixture that simultaneously acts as a plasticizer and as a viscosity regulator was added to all the mixtures. It had previously shown good interaction with EAFS, as this research team has reported in a previous study (Santamaría et al. 2020b). Water from the urban mains supply of the city of Burgos (Spain) was also added to all mixtures.

2.2. EAFS and natural aggregates

All the mixtures contained EAFS, the main physical properties of which were a density of 3.4 Mg/m^3, a water absorption level of 1.12 % and an angularity coefficient, as specified in BS-812 (British Standard Institution 1975), close to 11 units. This aggregate was crushed and sieved in two grading sizes, fine <4 mm (fineness modulus of 3.9 units) and medium 4/12 mm (fineness modulus of 5.7 units), and exposed to the outside environment for three months. In Figure 1, its granulometry curve is plotted. Table 1 shows its XRF chemical analysis results and the main crystalline components obtained by XRD. Additional characteristics of this aggregate may be consulted in previous studies by this research team (Ortega-López et al. 2018; Santamaría et al. 2020b).

The fines content of EAFS is markedly insufficient to produce high-workability mixes without segregation (Qasrawi 2018), so EAFS was combined with limestone 0/1.18 mm with a specific gravity of 2.65 Mg/m^3 and a fineness modulus of 1.5 units (Figure 1). The main limestone component was calcite (> 95 %).

Table 1. Chemical composition (XRF) and XRD analysis results of slag.

	Fe_2O_3	CaO	SiO_2	Al_2O_3	MgO	MnO	SO_3	Cr_2O_3	P_2O_5	TiO_2	Others (Na_2O…)	XRD results
LFS	1.0	59.2	21.3	8.3	7.9	0.3	1.4	0.0	0.0	0.2	0.4	Periclase; Olivine; Mayenite
EAFS	22.3	32.9	20.3	12.2	3.0	5.0	0.4	2.0	0.5	0.8	0.6	Wüstite; Ghelenite; Kirsteinite

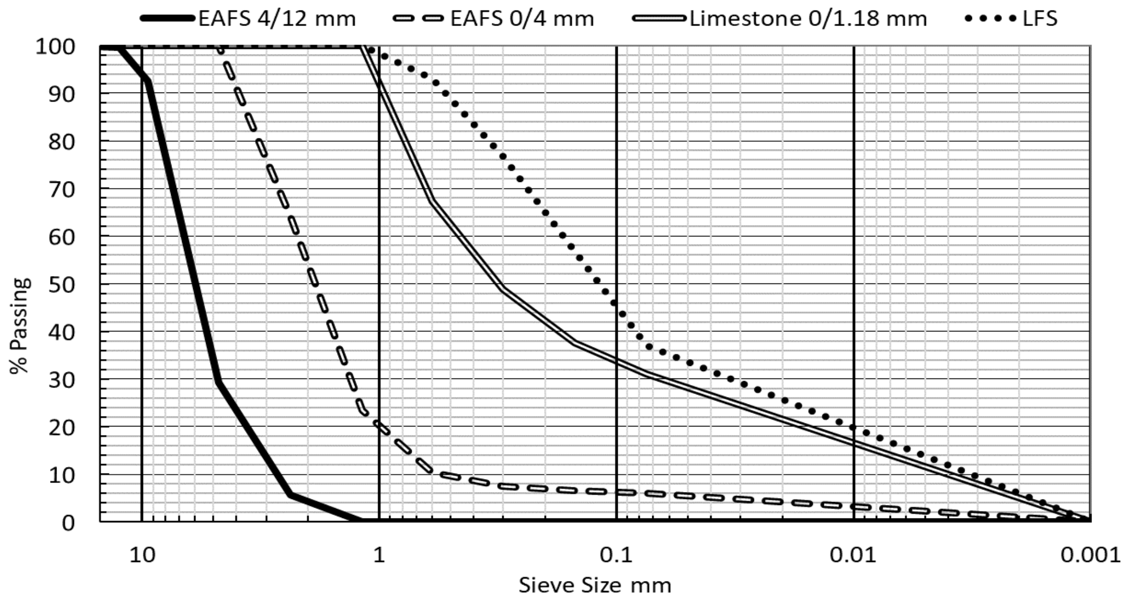

Figure 1. Aggregate gradation.

2.3. Fibers

Both metallic (M) and polymeric (Y) fibers were added to the mixtures, the characteristics of which are summarized in Table 2. Metallic fibers were hooked-end-shaped steel wire pieces. Polymeric fibers were surface dimpled, in order to maximize their adherence with the cementitious matrix (Tanaka et al. 2018).

Table 2. Physical characteristics of the fibers.

Type	Material	Length (mm)	Density (kg/m^3)	Young's modulus (GPa)	Tensile strength (MPa)	Equivalent diameter (mm)	Length/diameter aspect ratio
Metallic (M)	Steel	35	7,900	210	> 1,200	0.55	64
Polymeric (Y)	Polyolefin Polypropylene	35	910	6	> 400	0.93	38

2.4. Mix design

Four different mix designs were evaluated in this study. They represented different combinations of the two types of cement and fibers (0.5 % in volume of concrete mass) described earlier. All the mixtures incorporated 100 % EAFS with sizes of 0/4 and 4/12 mm, although limestone fines with a maximum size of 1.18 mm were also added as aggregate powder to improve workability (Santamaría et al. 2020a). Suitable proportioning of concrete mixes containing EAFS has been widely analyzed and described in previous works (Santamaría et al. 2020b). The concrete mixes were labelled *XC-F*:

- *X*. Cement type added: II (CEM II/B-S 42.5 N) or III (CEM III/B 32.5 N). Moreover, an amount of LFS equal to 6 % of the total binder content was combined with CEM III/B 32.5 N.
- *C*. Mix consistency: SC (self-compacting) or P (pumpable).
- *F*. Type of fibers used: M (metallic) or Y (polymeric). Mix IISC incorporated no fibers, so it can be considered the reference mixture. It is relevant to remember that the attainment of high-workability mixes is indispensable in the context of this work to perform an efficient structural concrete, which implies a fiber-content limitation at the proposed value of 0.5 %.

Regarding the mix design, the amount of binder was around 10 % of the total volume in all mixtures, the content of limestone fines was greater in self-compacting mixes to improve workability (35 % volume in self-compacting mixes and 25 % in mix IIIP-M), and the admixture content in no case exceeded 2 % of the cement mass, to avoid its segregation (Santamaría et al. 2017). The total amount of EAFS was around 40 % of the volume in self-compacting mixes, and 50 % in mix IIIP-M.

The slightly higher water content necessary to reach high workability when rough EAFS was mostly used as aggregate had to be increased to obtain that same workability when fibers were added to the concrete mix, which led to water-to-binder (w/b) ratios higher than 0.5 units. The interaction between the admixture and the large amount of slags (EAFS, LFS, GGBFS) prevented suitable self-compactability (presence of bleeding, segregation…) when CEM III/B 32.5 N was used, so an S4 consistency class as per EN 206 (EN-Euronorm) was defined as the target in this case.

Table 3. Mix design.

Component (Kg/m^3)	**IISC**	**IISC-M**	**IISC-Y**	**IIIP-M**
CEM II/B-S 42.5 R	330	330	330	-
CEM III/B 32.5 N	-	-	-	320
LFS	-	-	-	20
Water	170	180	185	160
Water-to-binder (w/b) ratio	0.52	0.55	0.56	0.45
EAFS medium (4/12 mm)	750	750	750	930
EAFS fine (0/4 mm)	550	550	550	690
Limestone fines (< 1.18 mm)	950	950	950	650
Admixture (% cement weight)	1.6	1.6	1.6	1.4
Fiber reinforcement	-	40	4.5	38
Total mass	2700	2740*	2705*	2780
*The total mass measurements correspond to a volume of 1030 liters.				

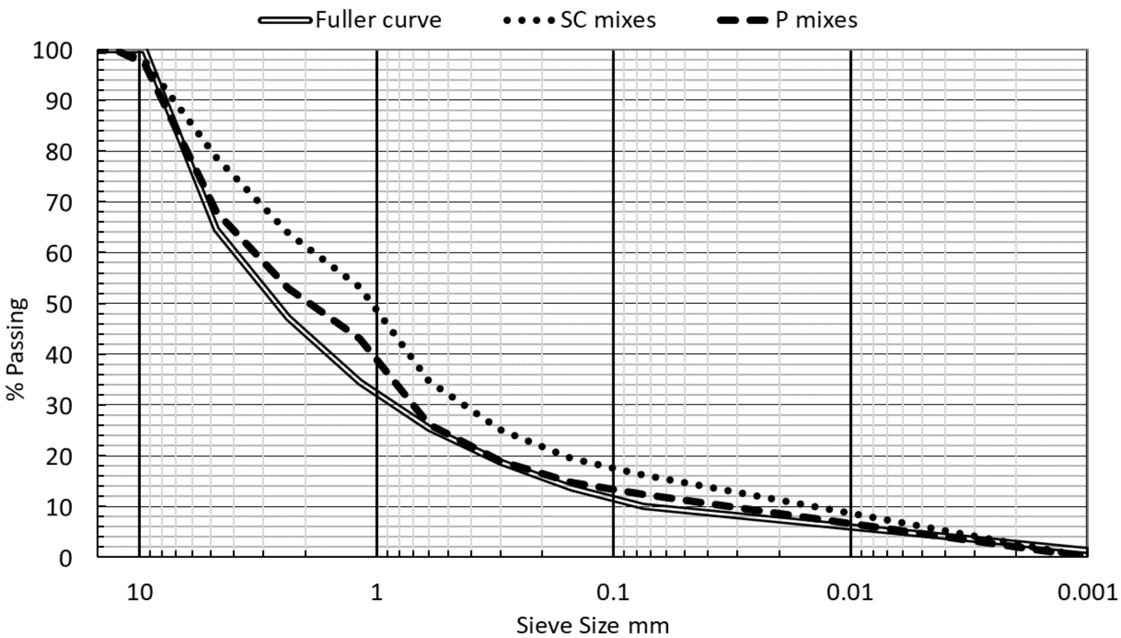

Figure 2. Global gradation of the mixtures.

The mix compositions are shown in Table 3. Their global granulometry is represented in Figure 2, in which their acceptable adjustment to the Fuller curve with 0.5 unit exponents can be observed; the inclusion of EAFS in self-compacting mixes usually leads to reduce it to around 0.45 units (Santamaría et al. 2020b).

2.5. Experimental plan

The mixing process took place in three stages to improve workability (Güneyisi et al. 2014). Firstly, the aggregates and water were added to the concrete mixer at outdoor-ambient humidity to achieve an optimal homogeneous distribution. In the second stage, the binder and the dissolved admixture were added. Finally, the fibers were included when the mix components had been suitably soaked and homogenized.

The slump-flow and L-box (self-compacting mixes), Abrams cone (pumpable mix), density, air content and setting (initial plastic shrinkage) tests were performed on samples of the fresh concrete mixtures. At the same time, several sample types were molded and subsequently cured in a moist room (humidity of 95 ± 5 % and temperature of 20 ± 2 °C) over various periods of time, before the hardened state tests. The final results were obtained by averaging the test results of three specimens. Table 4 shows the details of the samples and their testing.

Table 4. Hardened-state tests.

Test	**Age (days)**	**Standard** (EN-Euronorm)	**Samples**
Hardened density	28	EN 12390-7	100x200-mm cylindrical samples
Compressive strength	7, 28, 90, 180, 360	EN 12390-3	100x200-mm cylindrical samples
Modulus of elasticity	90	EN 12390-13	100x200-mm cylindrical samples
Poisson coefficient	90	EN 12390-13	100x200-mm cylindrical samples
Four-point bending	180	EN 83509 EN 83510	75x75x285-mm prismatic samples
Water penetration under pressure	90	EN 12390-8	150x300-mm cylindrical samples
Capillary porosity	180	UNE-83982 (2008)	100x100x100-mm cubic samples
Long-term shrinkage	From 1 to 200	EN 83318	75x75x285-mm prismatic samples
Accelerated aging (expansion)	120 to 180	Adaptation of the ASTM standard D-4792 (NLT-361 1991)	75x75x285-mm prismatic samples

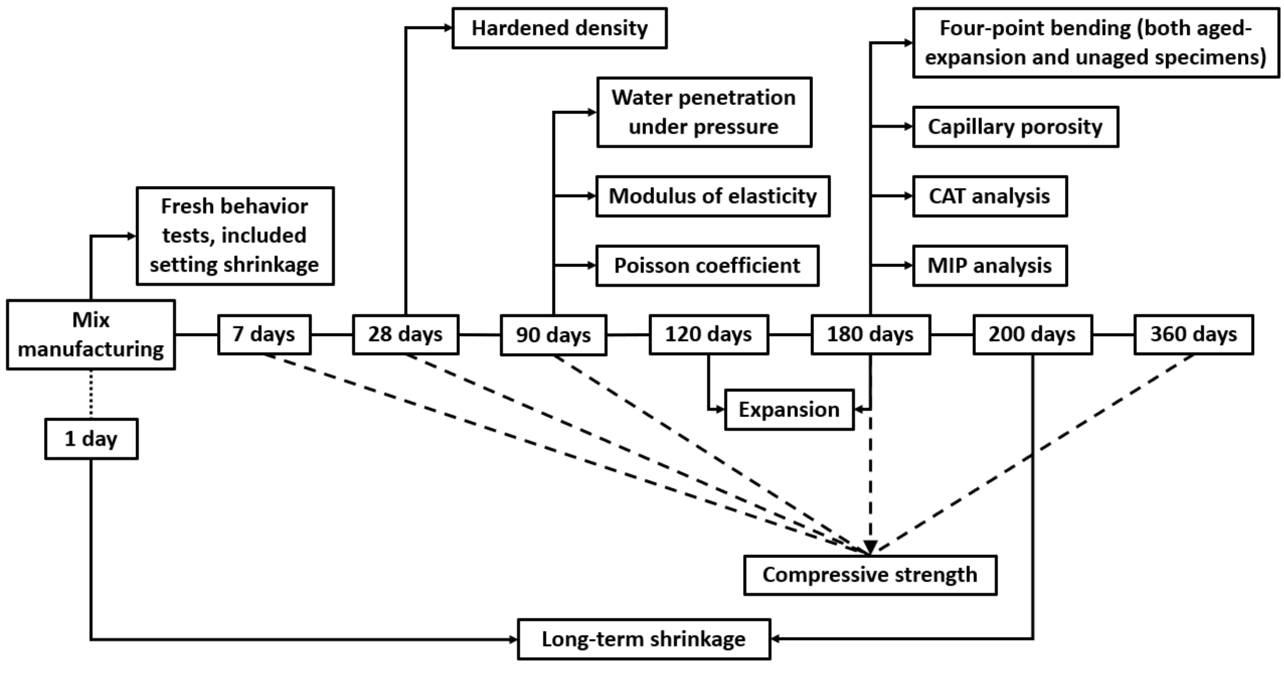

Figure 3. Experimental plan.

Mix porosity was also evaluated at 180 days using the Mercury Intrusion Porosimetry (MIP) analysis on fragments of the specimens from the compressive-strength test. X-ray Computed Tomography (XCT) analysis was performed on dog-bone shaped specimens of the mixtures. All the tests to evaluate mixture porosity were performed at the same concrete age, so that their results could be compared with each other (Wang et al. 2020). The microstructural analysis was completed by a Scanning Electron Microscopy (SEM) analysis.

Four-point bending tests were also performed on both unaged and aged specimens, in order to evaluate their pre- and post-aging strengths. In this way, the age of the concrete was not a parameter that influenced their fracture performance (De Domenico et al. 2018). All the properties that were tested and the experimental plan are shown in the flowchart of Figure 3.

3. Results and discussion

3.1. Fresh properties

The fresh properties of the mixtures were evaluated through the tests shown in Table 5. According to the test results, the self-compacting mixes made with CEM II/B-S had an SF1 and an SF2 slump-flow class for the mixtures with and without fibers, respectively. Mix IISC obtained a PA2 passing-ability class. The pumpable mix IIIP-M, made with LFS and cement III/B, reached a consistency of class S4. All these classifications followed the specifications in EN 206 (EN-Euronorm).

Table 5. Fresh tests results (consistency class in brackets).

Test	**Regulation** (EN-Euronorm)	**IISC**	**IISC-M**	**IISC-Y**	**IIIP-M**
Slump flow (mm)	EN 12350-8	720 (SF2)	650 (SF1)	620 (SF1)	-
Blocking ratio (3-bars L-box test)	EN 12350-10	0.82 (PA2)	-	-	-
Slump (mm)	EN 12350-2	-	-	-	175 (S4)
Air content (%)	EN 12350-7	2.3	2.1	1.8	3.5
Fresh density (Mg/m^3)	EN 12350-6	2.72	2.68	2.61	2.72

The slump flow was obtained as the average of two perpendicular spreading diameters and was reduced by the addition of fibers. Mix IIIP-M showed a correct pumping capacity (slump of 175 mm), despite its fiber content. Mix IISC showed an adequate ability to pass between the concrete reinforcement bars.

The fresh density was between 2.60 and 2.70 Mg/m^3; the higher density of EAFS compared to natural aggregate led to these values (Santamaría et al. 2020b). The air content, a measurement of spherical or vacuolar porosity, was around 2 % in the mixes with self-compactability. However, the air content reached 3.6 % in mix IIIP-M. This increase can be explained by the singular interaction between the LFS, the high content of GGBFS added to CEM III/B and the admixture, which favored the appearance of small spherical pores (Golestani et al. 2015).

3.2. Compressive tests (strength and stiffness) and hardened density

The main mechanical properties of the mixes are shown Figure 4 and Figure 5. Compressive strength was evaluated over one year through three samples breakage tests, while the modulus of elasticity, and Poisson's coefficient were also determined at 90 days for three samples.

Two groups of mixtures were categorized on the basis of the development of their compressive strength: CEM III/B pumpable mixes, and the CEM II/B-S self-compacting mixes. The strengths of the self-compacting mixes were greater, reaching values of between 45 and 60 MPa at 28 days, while the massive presence of GGBFS binder in mix IIIP-M inevitably lowered its compressive strength to 27.5 MPa at the same age. Moreover, the strength development of each group also differed (Figure 4). Mix IISC had the fastest strength development (at 90 days, it had reached 96.6 % of its strength at 360 days) and the fiber-reinforced self-compacting mixes, at 90 days, reached 92.4 % (IISC-M) and 93.9 % (IISC-Y) of their strength at 360 days. However, mix IIIP-M, at 90 days, had only reached 78.9 % of its strength at 360 days. The addition of LFS and high amounts of GGBFS therefore delayed the acquisition of compressive strength (Sideris et al. 2018).

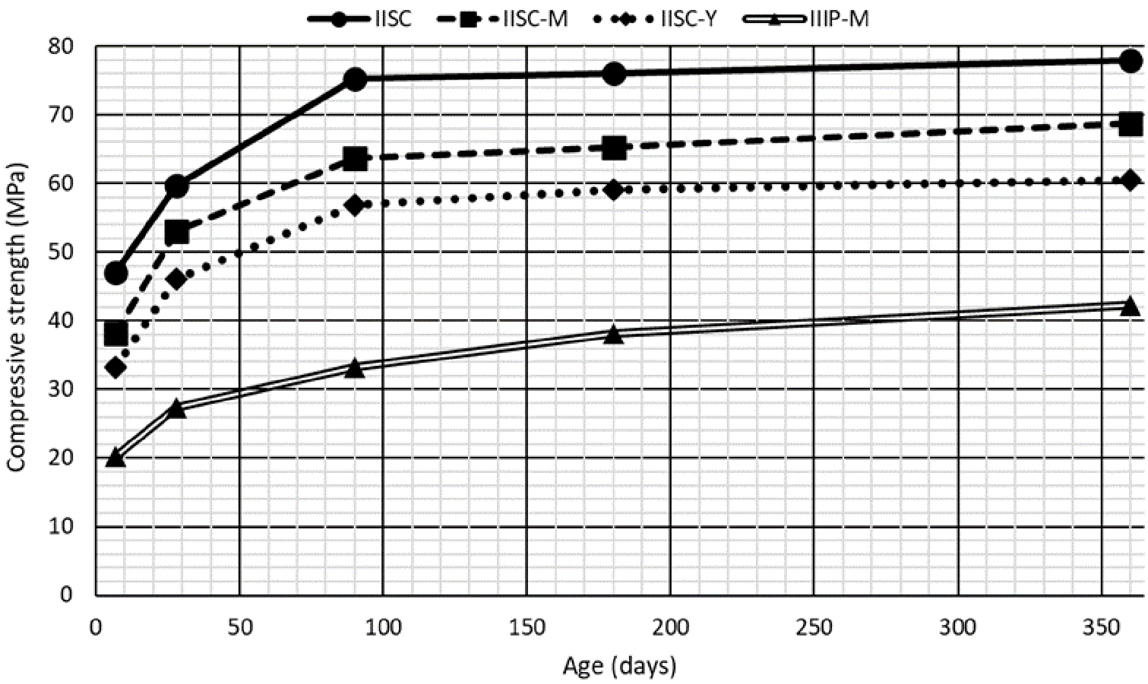

Figure 4. Compressive strength evolution.

This trend was also observed for the modulus of elasticity (Figure 5): mix IISC, the one with greater strength, presented the highest modulus of elasticity, 40.1 GPa, while the modulus of elasticity for mix IIIP-M was only 26.1 GPa. As deformability in the longitudinal direction increased, the transversal stiffness also increased (Fuente-Alonso et al. 2017): Poisson's coefficients of 0.23 for IISC and 0.19 for IIIP-M were obtained.

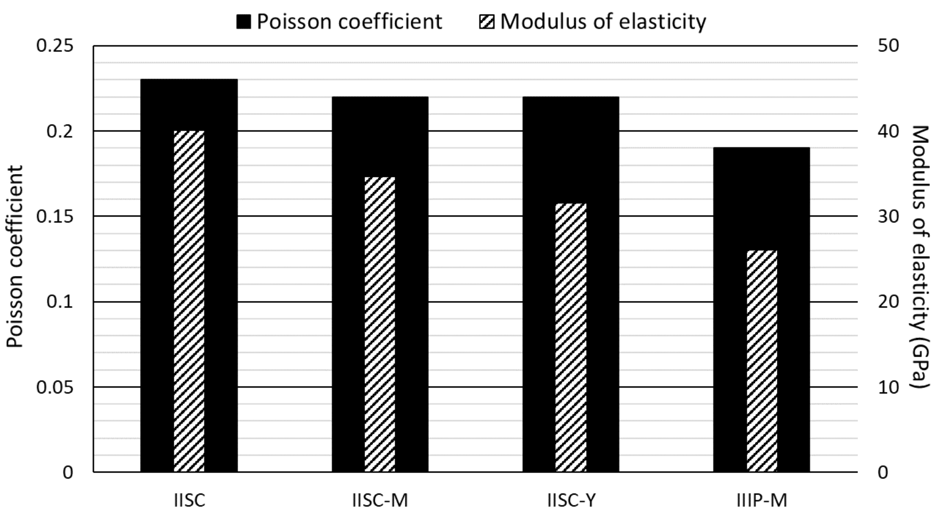

Figure 5. Modulus of elasticity and Poisson's coefficient at 90 days.

Finally, the hardened density at 90 days was between 2.54 and 2.65 Mg/m^3 for all the mixtures (2.63 Mg/m^3 for IISC mix, 2.57 Mg/m^3 for IISC-M, 2.54 Mg/m^3 for IISC-Y, and 2.65 Mg/m^3 for IIIP-M). The density values were higher than those obtained in conventional concrete due to the high density of EAFS (González-Ortega et al. 2019).

3.3. SEM analysis

Adherence between the different components of the mixtures (EAFS, fibers, and cement paste) and their Interfacial Transition Zone (ITZ) was evaluated using low-vacuum Scanning Electron Microscopy (SEM).

Images of breaking surface of some fragments from the compressive-strength tests on specimen mixes IISC-M (Figure 6) and IISC-Y (Figure 7) were examined.

Figure 6a shows a set of metal fibers embedded in the cementitious matrix, and the presence of matrix fragments adhered to fibers following breakage revealed good unions between the fibers and the matrix. Furthermore, the excellent quality of the hydrated cement matrix obtained with CEM II/B-S can be observed in the fractography of Figure 6b, where the surface is homogeneous without cracks and ridges.

In an effort to explain the low strength of the IISC-Y mixture compared with the IISC mixture, it was decided to evaluate the adhesion of EAFS particles sized between 1 and 4 mm to the cement paste. Both in Figure 7a and Figure 7b, it can be seen that no slippage of the ITZ occurred during the compressive tests, the EAFS particles having properly embedded themselves within the cementitious matrix.

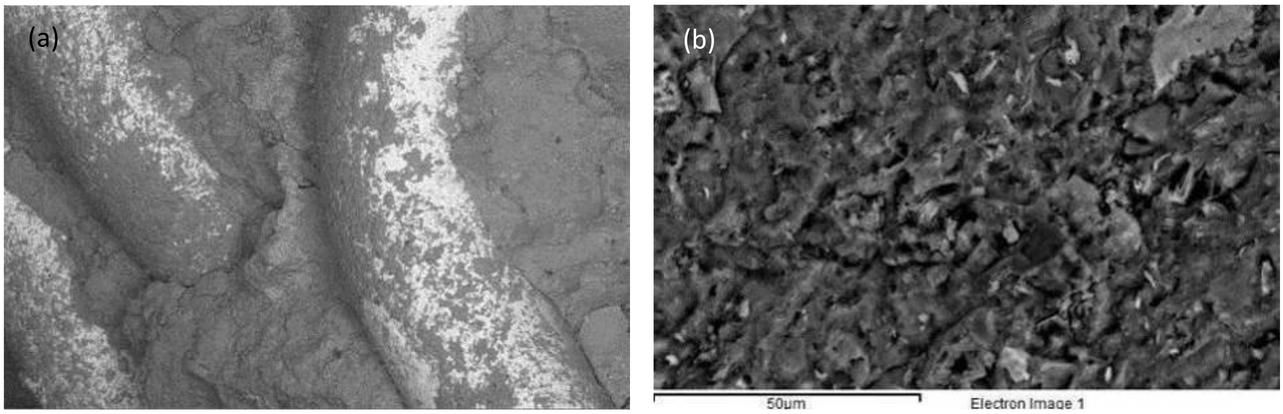

Figure 6. SEM images of mix IISC-M.

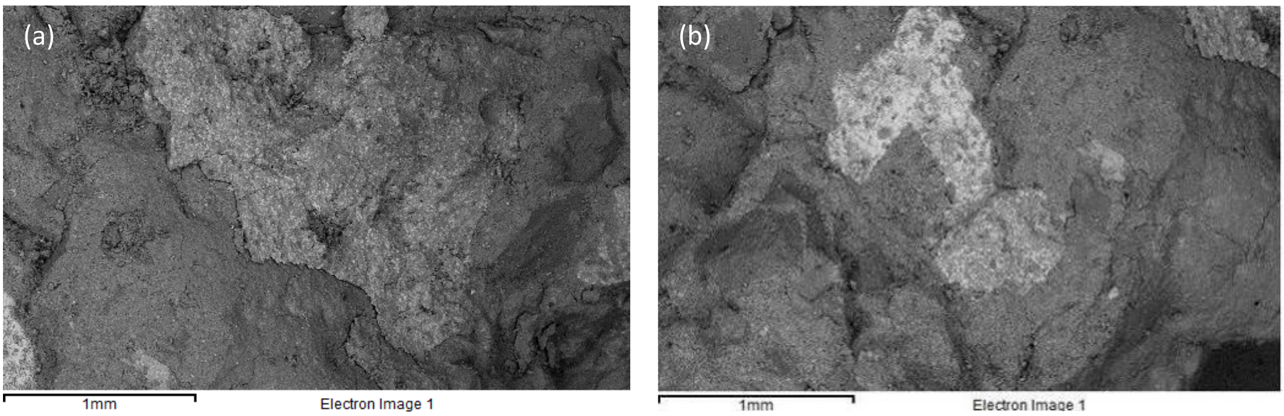

Figure 7. SEM images of mix IISC-Y.

3.4. Spontaneous dimensional variations assessment

The dimensional stability of the mixtures was studied through three different tests: setting shrinkage, long-term shrinkage and accelerated aging. The study was initially focused on the spontaneous or natural dimensional changes.

3.4.1. Setting shrinkage

The setting shrinkage (also called pre-setting shrinkage or plastic drying shrinkage) is an irreversible phenomenon that has been explained in detail elsewhere (Aragón et al. 2019). The test consists of arranging a sample of fresh concrete in an 800-mm-length gutter, in which the section is an inverted trapezium that is 50 mm in height and with a width of 50 at the bottom and 80 mm at the top. A fresh concrete portion was introduced in the gutter immediately after mixing and, during the setting (initial hours), could freely move at only one end, while the other end was fixed. The contraction (shrinkage) of the concrete was recorded with a digital comparator. The arrangement of this test can be seen in Figure 8. The four mixtures under study were tested under laboratory conditions (temperature of 20 ± 2 ºC and humidity of 60 ± 5 %) for up to three days after their manufacture. Figure 9 shows the setting shrinkage curves over 3 days.

Figure 8. Arrangement of setting shrinkage test.

According to the results after three days, two groups of mixtures could be distinguished: the self-compacting mixes and the pumpable mix.

- The self-compacting mixes had a setting shrinkage of between 0.9 and 1.1 mm/m after three days. Both fiber types, especially the metallic ones, with a higher stiffness, worked as rigid elements that slightly lessened any shortening of the concrete (Ortega-López et al. 2018), mix IISC-M experiencing the least shrinkage. The posterior evolution in all these mixtures was similar: approximately 90 % of total shrinkage occurred during the first 6 hours; then, there was a stabilization period of up to 20 hours. Finally, the shrinkage increased by ±0.1 mm/m until the end of the test, from 24 to 72 hours; this last stretch corresponded to the onset of long-term "drying shrinkage" in the hardened state. Therefore, the "time zero" of long-term shrinkage was around 24 h.
- Mix IIIP-M had a setting shrinkage of 0.45 mm/m, approximately 50 % less than the SC mixtures. In addition, two aspects of its evolution differed. Firstly, the shrinkage in the first 6 h was slower (lower slope of the curve). Secondly, there was hardly any stabilization step, because the long-term drying shrinkage started immediately at a level of 0.4 mm/m from 6 to 72 h and at a rate of 0.0008 units per hour. A result that the massive presence of GGBFS in the binder of mix IIIP-M and the presence of fibers and the presumably expansive tendency of the LFS all help to explain. The influence of the cement type appears clear in this irreversible phenomenon, mainly due to its quality and grinding fineness, added to other variables that could in each case be advanced.

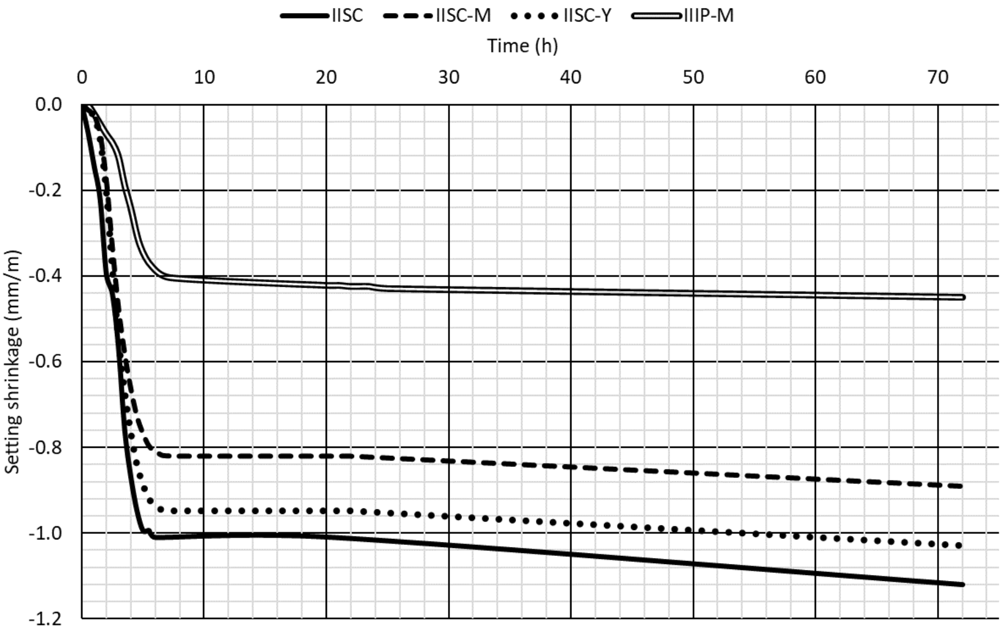

Figure 9. Setting-shrinkage test. Evolution over 3 days.

3.4.2. Long-term/drying shrinkage

Although the former setting/plastic irreversible shrinkage of concrete that occurs immediately after mixing is very important, this new circumstance, known as long-term/drying shrinkage, also occurs in an irreversible way throughout its life (Revilla-Cuesta et al. 2020a). Therefore, it is also fundamental to analyze the long-term shrinkage based on the loss of water of the hydrated calcium silicate gel.

Long-term concrete shrinkage was evaluated using 75x75x285-mm prismatic specimens, in accordance with EN 83318 (EN-Euronorm). Three specimens per mixture were kept in a dry room at 50 % relative humidity and at a temperature of 20 °C one day after mixing. Over 200 days, their length variation was controlled with a 300-mm frame equipped with a micrometer of a precision of 0.001 mm. The period between measurements depended on the length variation rate. Figure 10 represents the average length variations of the four concrete mixtures.

The long-term shrinkage results of the different mixes showed some similarities with the initial setting shrinkage, although there was also a remarkable difference: the shrinkage of mix IISC-M was closer to the value of mix IIIP-M, both reasonable values in themselves; those of the other self-compacting mixes (IISC and IISC-Y) were slightly high. If the values obtained for short-term and long-term shrinkage are compared, it can be observed that the plastic/setting shrinkage was 1.2-1.3 times greater than the long-term shrinkage values for the self-compacting mixes, while it was only 0.7 times for the pumpable mix IIIP-M.

- Regarding the self-compacting mixes, the steel fibers added to the concrete mixture reduced the long-term shrinkage value from mix IISC to mix IISC-M by 19 %. Nevertheless, this effect was not appreciated when polypropylene fibers were incorporated in the mixture (0.86 mm/m for mix IISC-Y), due to their low stiffness, their long-term viscoelastic properties, and the high w/b ratio of the IISC-Y mixture. The conclusions of similar studies also coincided in as much that polymeric fibers were less effective at lessening long-term shrinkage than metallic ones (Yousefieh et al. 2017).
- The long-term shrinkage value for mix IIIP-M was 0.65 mm/m, a value that is the global result of the concurrence of a wide set of factors. On the one hand, the presence of a stiff coarse aggregate (EAFS) in a larger proportion than in the other mixtures. On the other hand, the addition of slightly expansive LFS and the presence of metallic fibers restraining the lengthening. Furthermore, the use of less strong-stiff binder, with a high GGBFS content, and the lower w/b ratio also conditioned the final result.

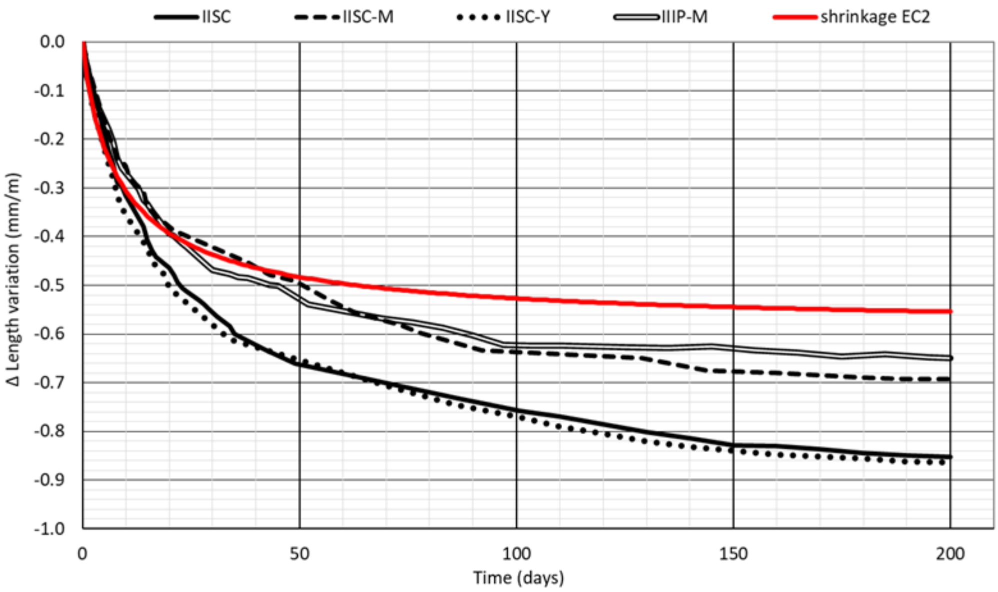

Figure 10. Long-term shrinkage of concrete mixtures.

The comparison between the experimental long-term-shrinkage values and the generic values of the EC-2 (2010) model (red color) is also represented in Figure 10. This model clearly underestimated the long-term shrinkage that occurred for all mixtures, except over the first 10 days. The reasons for this underestimation are probably based on the presence of SCM and the high content of EAFS as aggregate (Ortega-López et al. 2018). As stated in recent works, concretes containing EAFS usually show higher shrinkage rates than the concretes with natural aggregates (Santamaría et al. 2018). Moreover, the presence of pozzolanic additions (for example, fly ash or GGBFS) can also increase shrinkage (Santamaría et al. 2016). Nevertheless, all the concretes under study showed long-term shrinkage values lower than 0.9 mm/m, which is an acceptable value for structural concretes used in building and civil works (EC-2 2010; Salcedo and Fortea 2020).

3.4.3. Total shrinkage

The total shrinkage of the mixtures was calculated by adding the values of the setting shrinkage during the first 24 hours and the long-term shrinkage. The values obtained were in line with the value of each individual shrinkage: 1.87 mm/m for mix IISC, 1.51 mm/m for IISC-M, 1.81 mm/m for IISC-Y and 1.08 mm/m for IIIP-M. Total shrinkage values of well-performed structural concrete mixes are in the order of 1.5 mm (0.9 mm in the short-term and 0.6 mm in the long-term shrinkage) and are commonly accepted in building engineering.

3.5. Porosity/permeability assessment

In this section, the porosity/permeability of the mixtures and their test results are discussed.

3.5.1. Water penetration under pressure

The water penetration under pressure test cannot accurately determine concrete porosity, although it can compare the water permeability of the different mixtures. Despite the imprecise results frequently obtained in this test, the worst results are commonly obtained for the more permeable mixtures (Santamaría et al. 2018). The results for the mixtures of this study, performed on samples after 90 days of curing in moist room, are shown in Figure 11 after tests conducted in accordance with EN 12390-8 (EN-Euronorm).

In general, the incorporation of either metallic or polymeric fibers affected resistance to water penetration in a slightly negative way. However, the values of the self-compacting mixes were duplicated in mix IIIP-M, which showed a higher porosity and achieved higher pore connectivity, although mix IIIP-M met the standard specifications for less severe environmental exposures (maximum and average thresholds of 50 mm and 30 mm, respectively).

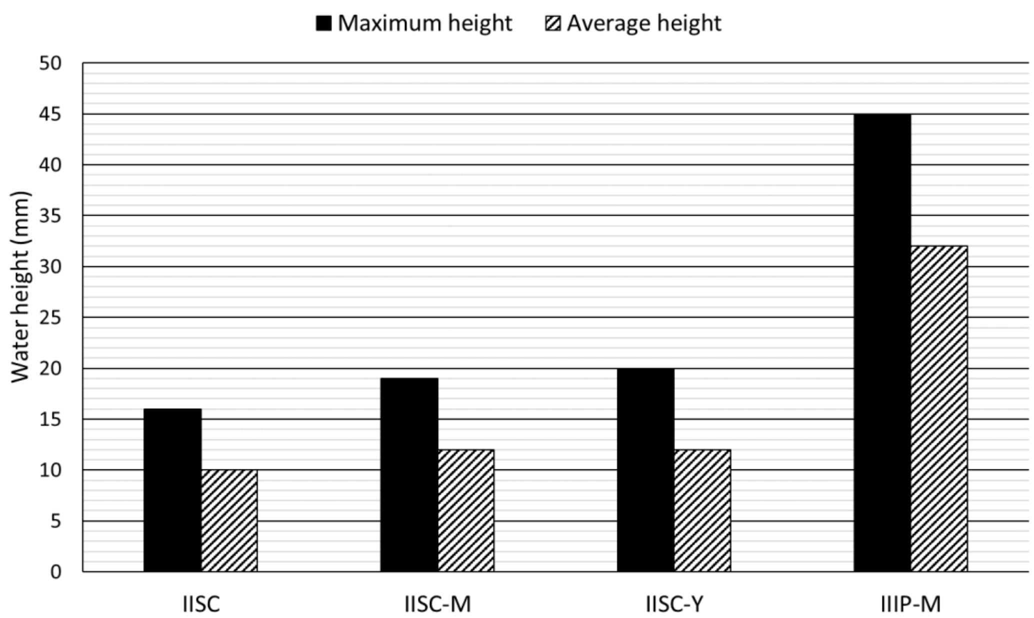

Figure 11. Water height in water penetration under pressure test.

Table 6 contains the results in terms of area, and maximum and average depth of water penetration in the mixtures. The permeability results of the self-compacting mixes (IISC, IISC-M, IISC-Y) were within the range of low-permeability concretes, showing maximum and average values lower than 25 mm and 15 mm, respectively, thereby complying with standard thresholds for impermeable concretes in any type of environmental scenario, which are established at values of 30 mm and 20 mm, respectively (EC-2 2010).

Table 6. Water penetration. Standard deviation between brackets.

Area (mm^2)	1031 (178)	1305 (283)	1337 (452)	4939 (822)
Maximum (mm)	16 (6.1)	19 (5.4)	20 (4.7)	45 (6.0)
Average (mm)	10 (4.5)	12 (4.8)	12 (5.1)	32 (12.8)

3.5.2. Mercury Intrusion Porosimetry (MIP) analysis

Without any doubt, MIP analysis is the best option for accurate measurement of the overall porosity of a cementitious mixture, because it measures the volume of capillary pores, their connectivity and size distribution (Santamaría et al. 2020a). MIP analysis was performed on specimen fragments from the compressive-strength tests at 180 days. An Autopore IV 9500 apparatus operating at a pressure of 33,000 psi recorded the MIP test results shown in Table 7, and Figure 12 presents the pore size frequency of the mixtures in terms of differential and cumulative volume intrusion.

Table 7. MIP analysis results.

		IISC	IISC-M	IISC-Y	IIIP-M
Total MIP porosity (% vol.)		9.5	12.3	13.4	14.7
Pore size distribution over total porosity (%)	**pore size < 20 nm**	11.4	10.5	10.7	32.5
	20 nm ≤ pore size < 50 nm	26.5	29.4	20.7	29.6
	50 nm ≤ pore size < 200 nm	36.0	30.2	32.5	6.8
	≥ 200 nm	26.1	30.0	36.1	31.1
Pore size distribution over the total volume of the mixture (%)	**pore size < 20 nm**	1.1	1.3	1.4	4.8
	20 nm ≤ pore size < 50 nm	2.5	3.6	2.8	4.4
	50 nm ≤ pore size < 200 nm	3.4	3.7	4.4	1.0
	pore size ≥ 200 nm	2.5	3.7	4.8	4.5
	≥ 200 nm (according to XCT analysis)	1.3	1.7	1.9	2.0
	MIP/XCT ratio (pores ≥ 200 nm)	1.92	2.18	2.53	2.30
Bulk density (Mg/m^3)		2.63	2.57	2.54	2.65

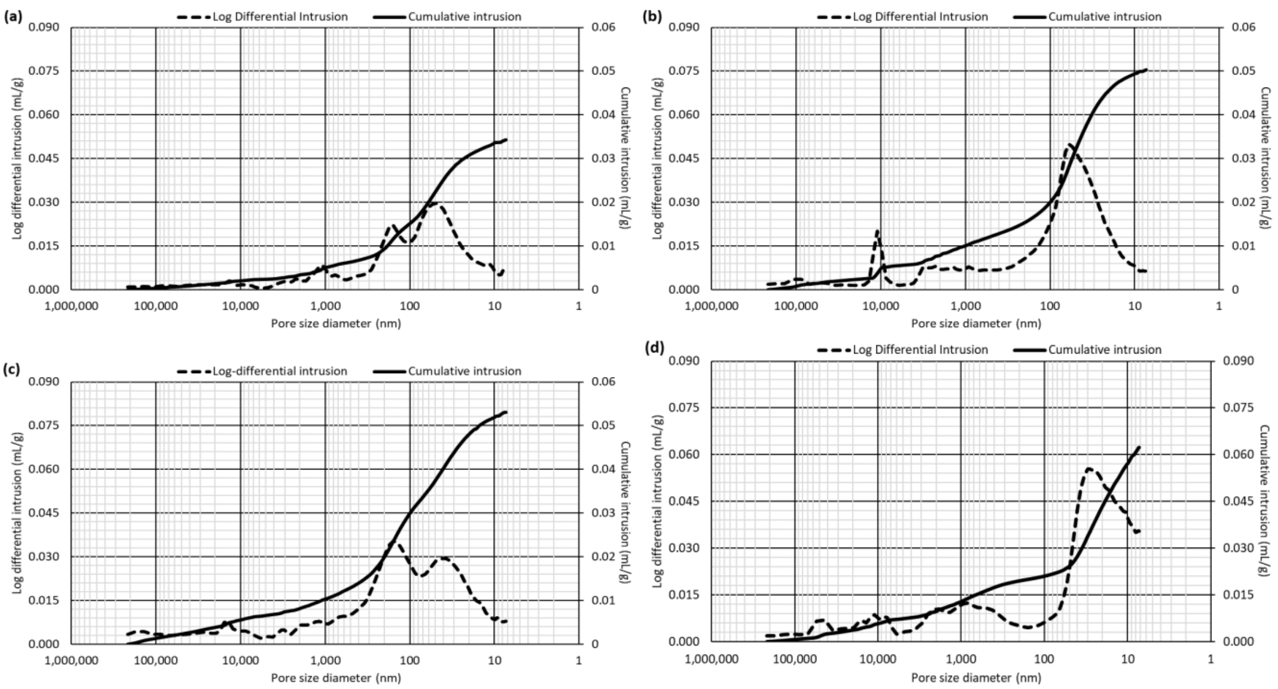

Figure 12. MIP pore size frequency in terms of differential and cumulative intrusion volume of the mixtures: (a) IISC; (b) IISC-M; (c) IISC-Y; (d) IIIP-M.

The total capillary porosity of the mixtures ranged between 9 and 15 %, in line with previous findings. These porosity levels were both proportional to the mix water, minus the water absorbed by the EAFS. Furthermore, the SCM and the fibers can be expected to increase porosity and pore connectivity (Santamaría et al. 2020a).

The lower porosity of the mixture without fibers, IISC (9.5 %), a more compacted concrete matrix than the others, explains its higher compressive strength (59 MPa at 28 days, 76 MPa at 180 days) and an eventual lower permeability of this mixture. The higher porosity of the fiber-reinforced self-compacting mixes, IISC-M (12.3 %) and IISC-Y (13.4 %), could mainly be attributed to their greater water-to-binder (w/b) ratio (Revilla-Cuesta et al. 2020a). The most abundant pore sizes in all the self-compacting mixes were concentrated at around 100 nm (matrix capillary porosity), a value that is the most favorable pore size for water diffusion (Ortega-López et al. 2018).

Mix IIIP-M was the mixture with the highest porosity, despite its lower w/b ratio. Furthermore, its pore size distribution differed notably from the self-compacting mixes: the most abundant pores were smaller than 20 nm (32.5 % of total pores, Table 7), while the pores of the self-compacting mixes were between 50-200 nm that represented the highest volume (30-36 % of the total pores). This result was partly due to the higher content of EAFS, which has a great micro-porosity in the range <200 nm, and partly due to the higher grinding fineness (specific surface) of the binder particles (GGBFS), which occluded a higher amount of <50 nm sized nano-bubbles during mixing. When the radius of an air cavity is smaller than the air cavities that the surface tension of the water-plasticizer-air system produces, their resemblance to perfect spheres progressively diminishes and they form part of the general capillary porosity.

Finally, the hardened (bulk) density test values depended on both the proportion of EAFS and the pore volume (Santamaría et al. 2020b); the pumpable mix, IIIP-M, had the highest density due to its higher EAFS content, followed by mix IISC.

3.5.3. Capillary water absorption test

The microstructural characteristics of the mixtures were also evaluated with the analysis of capillary absorption. Unlike the MIP analysis outlined above, this test uses water to determine concrete permeability, which is an indirect measure of porosity and pore connectivity.

Capillary porosity tests were performed on 100 mm cubic samples, cured for 180 days in a moist room, and then oven dried, as specified in UNE-83982 (2008) *"Determination of the capillary suction in hardened concrete. Fagerlund method"*. After adequate preconditioning, the samples were placed on a plate filled with water at a constant level of 5 ± 1 mm throughout the experiment. The test is considered to end when there is no further absorption of water in two consecutive daily measurements. The results are shown in Table 8, in which the classical units (cm, g) of permeability tests based on Darcy's law are used. The following results were obtained: water absorption gain (g); saturation time (t); resistance to water penetration by capillary absorption, inverse to speed (m); effective porosity that can be occupied by water (ε_e); and the coefficient of capillary absorption, a global characteristic of the permeability process (*K*). The results are shown in Figure 13, in terms of mass gain per unit area of the sample over the square root of time. A lower slope of the curve (measured by the *K* coefficient) before saturation indicates lower concrete permeability levels.

The results of effective porosity in Table 8 (ε_e) were consistent and lower than the porosity obtained in MIP analysis. MIP total porosity and the effective porosity, ε_e, were in proportions of around 1.25-1.35 units, which means that the mixtures contained certain initial moisture levels (25-20 %) and/or that there was an important volume of isolated pores without connectivity (Koenig 2020).

The effective porosity (ε_e) of the fiber-reinforced mixes IISC-M and IISM-Y increased with regard to IISC; this fact was attributed to the increased w/b ratio that fibers demand when added to a mixture (Fuente-Alonso et al. 2017). Moreover, IIIP-M was the mixture with the highest effective porosity; its capillary absorption coefficient (*K*), evaluated from the slope of the corresponding IIIP-M curve as depicted in Figure 13, can be associated with its higher proportion of capillary pores.

Moreover, the percentage of pores <20 nm (32.5 % of total porosity), according to MIP analysis, was much higher in mix IIIP-M than in the self-compacting mixes (around 10.5 %). As mentioned, these small pores are likely to be more interconnected than the larger ones (Koenig 2020). The results were in line with the ratio of occluded air and the resistance to water penetration under pressure, a test that lasts long enough to register slow water diffusion (sections 3.1 and 3.5.1).

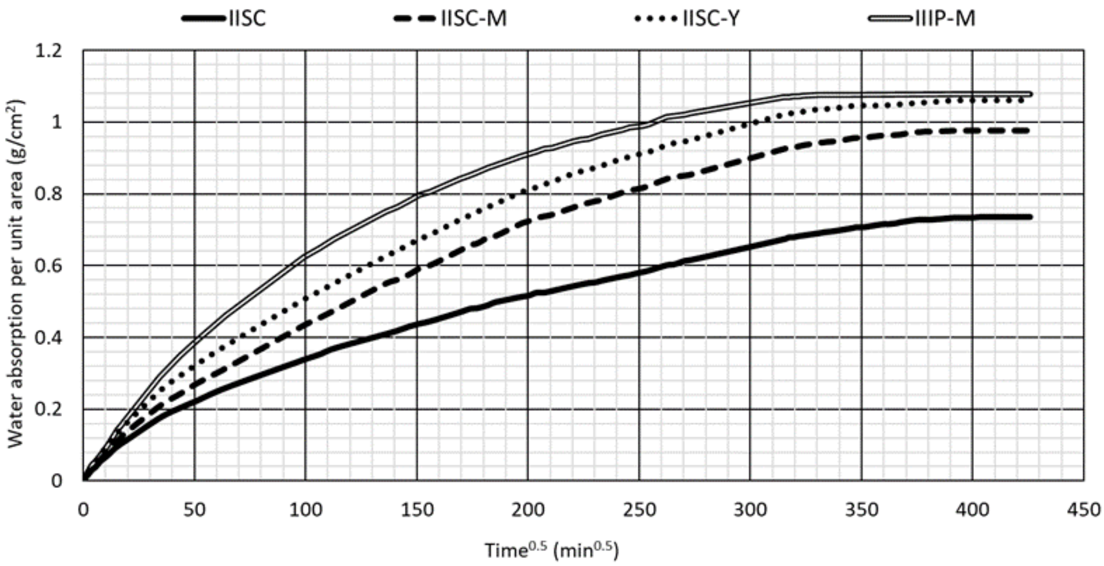

Figure 13. Capillary water absorption per unit of area versus square root of time (sqrt).

Table 8. Capillary porosity test results.

	IISC	IISC-M	IISC-Y	IIIP-M
g: water absorption by surface capillarity (g)	73.7	97.6	106.0	107.8
t_n: time of saturation (h)	2,344	2,160	1,927	1,760
sqrt t_n ($min^{0.5}$)	375	360	340	325
m: resistance to water penetration by capillary absorption (min/cm^2)	1,406	1,296	1,156	1,056
ε_e: effective porosity of concrete (cm^3/cm^3)	0.074	0.098	0.106	0.108
K: capillary absorption coefficient ($g/m^2{\cdot}min^{0.5}$)	14.3	19.1	21.7	23.7
ε_e: effective porosity of concrete (%)	7.4	9.8	10.6	10.8
ε_e: capillary porosity of concrete according to MIP analysis (%)	9.5	12.3	13.4	14.7
MIP/ε_e ratio (MIP porosity, effective porosity)	1.28	1.26	1.26	1.36

3.5.4. X-ray Computed Tomography (XCT) analysis

In an initial approximation, the mixture macrostructures were evaluated by XCT analysis on dog-bone shaped specimens after 180 days in a moist room; these specimens had also been used for tensile strength evaluation in another work of authors (Ortega-López et al. 2021). The mix components can be divided into four phases, due to their different densities (Table 9):

- EAFS metallic steel inclusions and metallic fibers: density close to 8 Mg/m^3.
- EAFS: density around 3.5 Mg/m^3.
- Cementitious matrix components (limestone fines, cement, LFS): density around 2 Mg/m^3.
- Air and polymeric fibers: low density between 0 and 0.9 Mg/m^3.

Table 9. Volume of each component of the concretes obtained with XCT analysis and occluded air.

Component (% vol.)	IISC	IISC-M	IISC-Y	IIIP-M
Steel inclusions, metallic fibers	0.5	1.3	0.4	1.2
EAFS	40.2	39.1	36.5	48.0
Cementitious matrix	58.0	57.9	60.7	48.8
Air and/or polymeric fibers	1.3	1.7	2.4	2.0
Air (porosity)	1.3	1.7	1.9	2.0
Occluded air (Table 5)	2.2	2.0	1.9	3.6

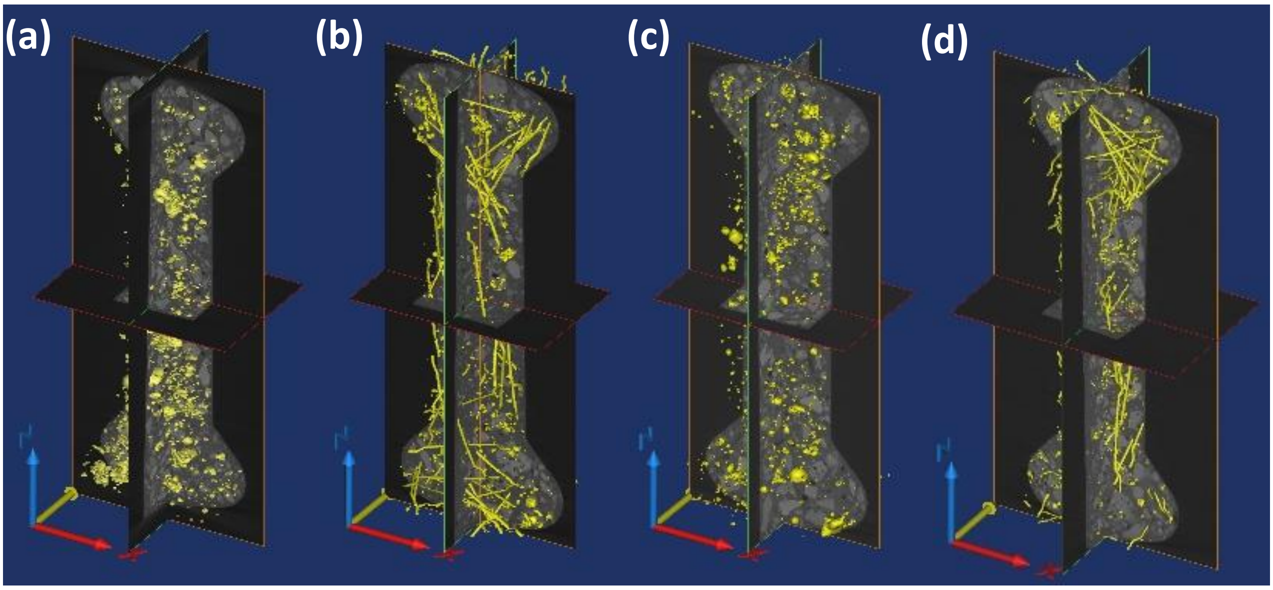

Figure 14. XCT images of metallic phase volume: (a) IISC; (b) IISC-M; (c) IISC-Y; (d) IIIP-M.

As an example, Figure 14 shows the metallic phase present in all the mixtures. Mix IIIP-M had a poorer distribution of the metallic fibers than mix IISC-M, which could favor the appearance of voids (Fuente-Alonso et al. 2017). In mixes IISC and IISC-Y, the metallic phase only affected steel remnants encrusted within the EAFS, with a volume fraction of around 0.5% of concrete, Table 9. However, in the steel-fiber-reinforced concretes, IISC-M and IIIP-M, this phase also included a volume of steel fibers (around 0.5% in volume of concrete as a theoretical value), which in Table 9 represented around 1.3 % of the total volume of the mixture.

The volumes of EAFS were highly consistent with the mix design (section 2.4): around 40 % for self-compacting mixes and 50 % for mix IIIP-M.

Finally, as expected, the estimated volume of air was in general lower than the occluded air (pore sizes between 0.1 and 5 mm) of the fresh concrete, as shown in Table 5. This result was partly due to the pixel size of the XCT analysis (100 μm) that could only define pores larger than 170 μm (Santamaría et al. 2020a); the volumes of air were consistent with the previous results where mix IIIP-M contained the highest volume of occluded air. Furthermore, the air volume and the content of polymeric fibers (0.5 % vol.) of mixture IIISC-Y amounted to a total of 2.4 %.

3.6. Accelerated-aging (expansion) tests

As indicated in section 2.5, prismatic specimens measuring 75x75x285-mm that had been cured for 120 days underwent an accelerated-aging test, adapted from the test specified in standard ASTM D-4792 (NLT-361 1991). The aim of this test was to evaluate the dimensional stability of the mixtures at moderately high temperature, since all slag types (EAFS, GGBFS, and LFS) could expand at mild temperatures, due to free lime or free magnesia hydration (González-Ortega et al. 2019); the eventual appearance of flaking and cracks through which aggressive external agents can penetrate (Yang et al. 2019) is dangerous and must be considered as such. In principle, performing this test for a period of time equal to 7 days could be enough to evaluate any possible expansion of the slag; nevertheless, if within a week any expansion has not stabilized, the test should be continued until stabilization occurs (Montenegro-Cooper et al. 2019; Ortega-López et al. 2014). According to this statement, in this study the samples were submerged in hot water at a temperature of 72±2 °C for 30 days and then left at environmental temperature (22±2 °C) for another 30 days to evaluate any lengthening. Subsequently (at 180 days), the specimens underwent compressive strength and four-point bending tests as per EN 83509 and EN 83510 (EN-Euronorm). The results were compared with the results of identical specimens that had not undergone the aging test. The comparison served to evaluate the effect of accelerated aging on the strength of each mixture.

3.6.1. Dimensional variation. Internal damage

The length variations over 60 days of all the mixtures throughout the aging tests are shown in Figure 15. On the one hand, assuming that lengthening, in its first stage, corresponded to the thermal dilatation of the concrete, a subsequent lengthening of 0.18 mm/m from an initial value of around 0.65 mm/m to a final value of 0.83 mm/m was recorded for mix IISC during the heating period (0-30 days); the mixture hardly lengthened any further. On the other hand, mix IIIP-M underwent greater progressive lengthening over the same period in the presence of metallic fibers: an initial thermal strain of 0.70 mm/m and a final strain of 1.10 mm/m. In the same way, mix IISC-M presented a strain of 0.63 mm/m after six days of testing, while this value for mix IISC-Y was 0.75 mm/m. The final strain for both mixtures was around 0.98 mm/m.

All the mixtures underwent pronounced thermal contraction at room temperature on the first day of the second period of exposure (31-60 days) after which the final strain was between 0.15 and 0.30 mm/m. However, all the mixtures progressively decreased their strain levels over the 30 days of the second phase and, at the end of this period, they all underwent a slight and hardly significative lengthening. The mixtures with the highest strain levels during the heating phase were the ones with the highest remaining levels recorded at room temperature at the end of the exposure phase. Mix IISC had the lowest remaining strain (0.04 mm/m) after this period, while the values of the other self-compacting mixes were similar, in the order of 0.08-0.1 mm/m. Mix IIIP-M presented a final strain of 0.14 mm/m after the presumable expansion of LFS during the heating period.

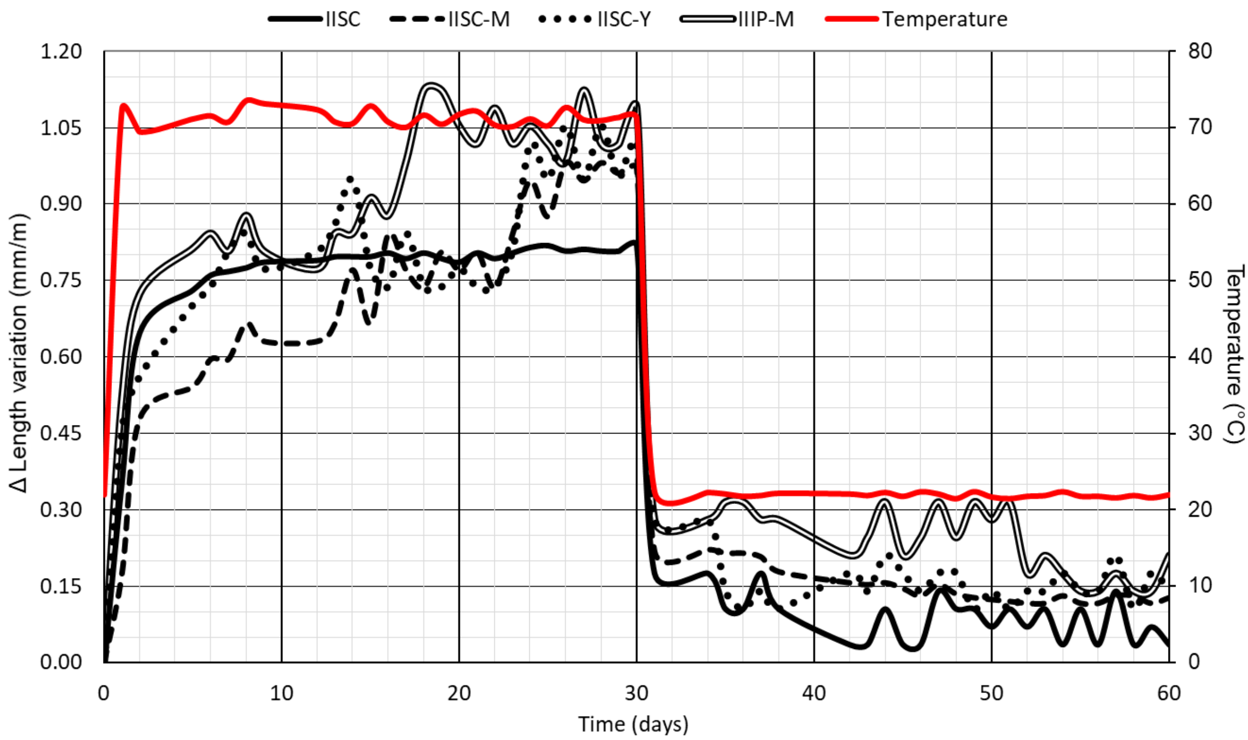

Figure 15. Strain evolution in the accelerated-aging test.

EAFS expansion causes very moderate lengthening in self-compacting mixes and neither flakes nor cracks were observed in any of the test samples (Figure 16); however the sample corners and edges were rounded, due to a slight loss of material. In addition, after the test, all the mixtures showed stains of a darker color, probably caused by chemical reactions of the slag during the water heating period (Kim et al. 2016). Finally, oxidation of the metallic fibers closer to the sample surface was also observed, which might potentially worsen the performance of concrete (Bernachy-Barbe et al. 2020).

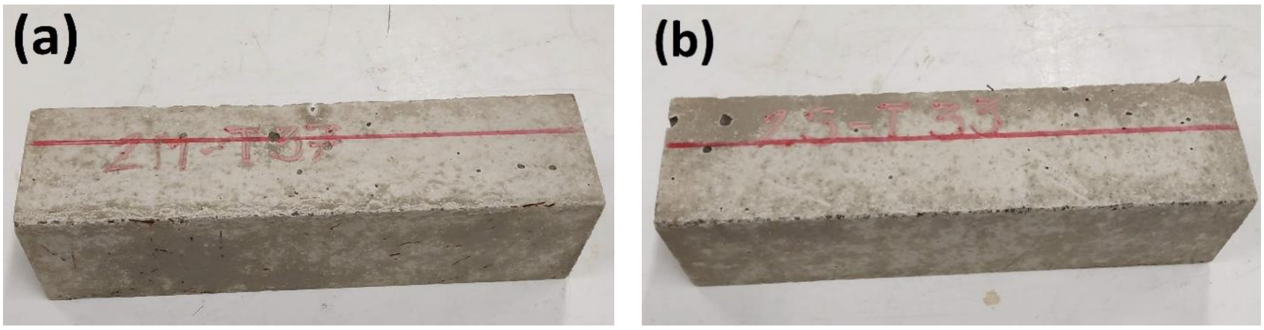

Figure 16. Samples 75x75x285 mm after accelerated-aging test: (a) IISC-M; (b) IISC-Y.

The damage to the concrete caused by the above-mentioned reactions could not be detected with the naked eye, so non-destructive measurements, such as the hardened density and the Ultrasonic Pulse Velocity (UPV), were performed both before and after the test. The results are shown in Table 10.

- A loss of density of between 0.8 and 1.5 % was observed in all the mixtures, indicating that hydration or carbonation reactions within the concrete are hardly probable. The loss of mass in submerged concrete is usually associated with the dissolution of Portlandite-Calcium Hydroxide in tempered water in the form of calcium bicarbonate and the final precipitation of calcite at the bottom of the tray. Furthermore, at the test temperature of 72 °C, it is plausible to assume a slight decomposition of primary ettringite with the loss of molecular water.
- The UPV test revealed an eventual internal damage of the cementitious matrix, such as the appearance of micro-cracks (Selleck et al. 1998). The initial values were in accordance with the previously detailed compressive strength and modulus of elasticity: the highest UPV values were obtained in mix IISC, and the lowest in mix IIIP-M. Furthermore, the high stiffness of the cementitious matrices contributed negatively to their integrity in the thermal lengthening and contraction processes: mix IIIP-M showed the least damage, so an UPV variation of only 0.7 % was recorded. In the rest of mixtures, the UPV losses ranged from -7 to -9 % clearly revealing internal damage.

Table 10. Hardened density and UPV before and after accelerated-aging test.

	IISC		**IISC-M**		**IISC-Y**		**IIIP-M**	
	Initial	**Final (Δ%)**	**Initial**	**Final (Δ%)**	**Initial**	**Final (Δ%)**	**Initial**	**Final (Δ%)**
Hardened density (Mg/m^3)	2.63	2.60 (-0.8)	2.57	2.54 (-1.2)	2.54	2.52 (-0.8)	2.65	2.61 (-1.5)
UPV (km/s), EN 12504-4 (EN-Euronorm)	3.99	3.68 (-7.8)	3.97	3.61 (-9.1)	3.89	3.60 (-7.5)	2.82	2.80 (-0.7)

3.6.2. Mechanical testing

After the accelerated-aging test at 72 °C (both heating and room temperature periods), the 75x75x285-mm specimens underwent four-point bending test and compressive strength tests (split into 75x75x75-mm cubic samples). At the same time (180 days), unaged specimens, up until then in the moist room, were tested in the same way to evaluate the effect of the accelerated-aging test on their flexural strength and the fracture behavior of the concrete. Figure 17 shows the load-deflection curves obtained in each case, while Table 11 shows the characteristic values of the tests. A limit deflection of 1.5 mm was established for its calculation according to EN 83510 (EN-Euronorm).

The results for the unaged specimens coincided with the previous compressive strength values. Mix IISC showed the greatest strength, although its brittle behavior after cracking was due to the absence of fibers (Larsen and Thorstensen 2020). The other mixtures presented lower strengths, but better performance after cracking. Mix IISC-Y, made with polymeric fibers, had the lowest fracture toughness and fracture energy (Park et al. 2019).

Table 11. Flexural toughness and post-cracking behavior of unaged mixtures and mixtures that underwent accelerated-aging tests.

	Unaged samples				Aged samples			
	IISC	**IISC-M**	**IISC-Y**	**IIIP-M**	**IISC**	**IISC-M**	**IISC-Y**	**IIIP-M**
Compressive strength	76.1	65.2	59.1	38.1	66.4	58.7	54.4	37.6
Flexural toughness (N·m)	4.27	10.45	4.09	4.82	1.60	10.03	3.46	5.31
First crack strength (MPa)	7.91	5.41	4.48	3.41	3.11	4.45	3.63	3.17
Fracture energy, G_F (N/mm)	0.754	1.86	0.727	0.857	0.278	1.828	0.614	0.944

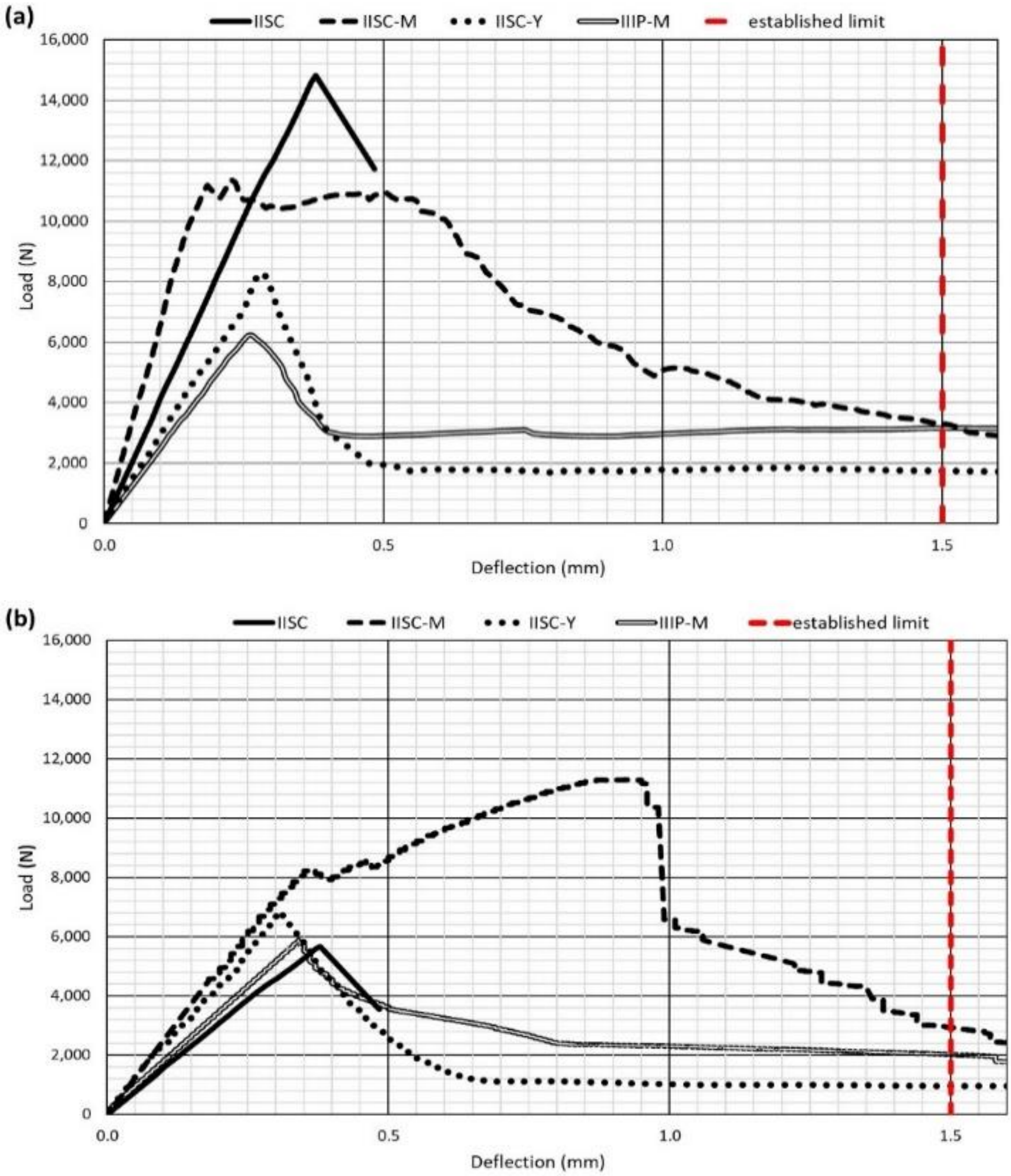

Figure 17. Load-deflection curves: (a) unaged samples; (b) aged samples.

After the accelerated-aging tests, the compressive strength results presented an appreciable decrease, and losses of ±10 % except for IIIP-M, in relation to the values given by similar tests on unaged specimens with the same curing period. Despite the presence of LFS, mix IIIP-M revealed no serious structural damage.

On the one hand, the behavior of the self-compacting mixes, with a cementitious matrix of high stiffness and strength, was negatively affected by thermal expansion, which had the worst effect on mix IISC, even though its lengthening was minimal. Consequently, its tensile stiffness-strength and fracture energy decreased after the accelerated-aging test, which can be observed in the initial segment of the load-deflection curve that is less steep, as shown in Figure 17. Moreover, its first crack strength and fracture energy decreased 57 % and

70 %, respectively. The addition of metallic fibers (mix IISC-M) caused a loss of stiffness after the accelerated-aging test, although its tensile strength decreased. The addition of polymeric fibers (mix IISC-Y) showed a similar behavior.

On the other hand, mix IIIP-M underwent the greatest residual lengthening in Figure 15. Nevertheless, it showed no internal damage (according to UPV and compressive values), and its flexural toughness and fracture energy increased. The eventual slight expansiveness of the slag appears not to have negatively affected the performance of this mixture. The greater compliance of its cementitious matrix allowed it to better withstand the internal stress resulting from thermal dilatation and LFS expansion (Roslan et al. 2020).

4. Conclusions

The mechanical properties of high-workability mixtures manufactured with fibers and slag aggregate and binder, their porosity-permeability, short- and long-term shrinkage and accelerated-aging have all been analyzed. In general, these high-workability concretes present higher porosity values and slightly greater shrinkage values than conventional concretes, due to their high volumes of mix water. If such mixtures also contain high quantities of slag as aggregate or SCM and low quantities of fibers, the nature of those materials will accentuate those properties. The following conclusions can be drawn.

- Self-compacting mixes were produced, simultaneously using large quantities of EAFS, 30 % GGBFS binder, and both metallic and polymeric fibers, after adjusting the w/b ratio.
- Nevertheless, the addition of 70 % GGBFS and 6 % LFS as proportions of the total binder content reduced workability, due to poor interaction between these slag types and the admixtures, and simultaneously deteriorates the mechanical properties. Mercury Intrusion Porosimetry (MIP) analysis indicated that pore volumes <50 nm also increased following additions of GGBFS and LFS.
- The increase in the w/b ratio necessary to achieve high workability when concrete has fiber additions produced an increase in porosity and lowered mechanical performance levels; having considered all advantages and inconveniences, the use of fibers in this kind of mixtures is inadvisable.
- Both X-ray Computed Tomography (XCT) analysis and the capillary porosity test tended to underestimate porosity, but both supply interesting data on mixture porosity.
- The setting/plastic shrinkage, measured up to 24 h after mixing, was approximately 25 % higher than the long-term shrinkage. The addition of polymeric and especially metallic fibers reduced both types of shrinkage, while the expansive characteristics of LFS were effective at reducing setting shrinkage and slightly reducing long-term shrinkage.
- All the mixtures showed small dimensional variation after accelerated-aging tests. The thermal variations caused internal stresses within the concrete, which resulted in the appearance of micro-cracking and a worsening of the pre- and post-cracking behavior according to the flexural-strength test results. Additions of GGBFS and LFS in large quantities generated a cementitious matrix of lesser stiffness and any expansive damage was practically null.

Acknowledgements

The authors wish to express their gratitude for funding this research work to: the Spanish Ministry MCI, AEI, EU and ERDF [PID2020-113837RB-I00; RTI2018-097079-B-C31; 10.13039/501100011033; FPU17/03374]; ERDF and the Junta de Castilla y León [BU119P17; UIC-231]; ESF and Youth Employment Initiative (JCyL) [UBU05B_1274]; the Basque Government research group SAREN; the University of The Basque Country [PPGA20/26]; and the University of Burgos [Y135.GI]. Our thanks also go to the companies Chryso Additives and Hormor-Zestoa for their ongoing collaboration with research group members.

Declaration of interest

The authors declare that there is no conflict of interest.

Data availability

All data, models, and code generated or used during the study appear in the submitted article.

References

European Association representing metallurgical slag producers and processors (EUROSLAG).

Abu-Eishah, S.I., A.S. El-Dieb, and M.S. Bedir. 2012. "Performance of concrete mixtures made with electric arc furnace (EAF) steel slag aggregate produced in the Arabian Gulf region." *Constr. Build. Mater.* 34: 249-256. https://doi.org/10.1016/j.conbuildmat.2012.02.012.

Afroughsabet, V., L. Biolzi, and T. Ozbakkaloglu. 2016. "High-performance fiber-reinforced concrete: a review." *J. Mater. Sci.* 51 (14): 6517-6551. https://doi.org/10.1007/s10853-016-9917-4.

Aragón, G., Á. Aragón, A. Santamaría, A. Esteban, and F. Fiol. 2019. "Physical and mechanical characterization of a commercial rendering mortar using destructive and non-destructive techniques." *Constr. Build. Mater.* 224: 835-849. https://doi.org/10.1016/j.conbuildmat.2019.07.034.

Arriagada, C., I. Navarrete, and M. Lopez. 2019. "Understanding the effect of porosity on the mechanical and thermal performance of glass foam lightweight aggregates and the influence of production factors." *Constr. Build. Mater.* 228: 116746. https://doi.org/10.1016/j.conbuildmat.2019.116746.

Bahramian, M., and K. Yetilmezsoy. 2020. "Life cycle assessment of the building industry: An overview of two decades of research (1995–2018)." *Energy Build.* 219: 109917. https://doi.org/10.1016/j.enbuild.2020.109917.

Bernachy-Barbe, F., T. Sayari, V. Dewynter-Marty, and V. L'Hostis. 2020. "Using X-ray microtomography to study the initiation of chloride-induced reinforcement corrosion in cracked concrete." *Constr. Build. Mater.* 259: 119574. https://doi.org/10.1016/j.conbuildmat.2020.119574.

Bondar, D., M. Basheer, and S. Nanukuttan. 2019. "Suitability of alkali activated slag/fly ash (AA-GGBS/FA) concretes for chloride environments: Characterisation based on mix design and compliance testing." *Constr. Build. Mater.* 216: 612-621. https://doi.org/10.1016/j.conbuildmat.2019.05.043.

Bosela, P., N. Delatte, R. Obratil, and A. Patel. 2009. "Fresh and hardened properties of paving concrete with steel slag aggregate." *Carreteras* 4 (166): 55-66.

Branca, T.A., V. Colla, D. Algermissen, H. Granbom, U. Martini, A. Morillon, R. Pietruck, and S. Rosendahl. 2020. "Reuse and recycling of by-products in the steel sector: Recent achievements paving the way to circular economy and industrial symbiosis in europe." *Metals* 10 (3): 345. https://doi.org/10.3390/met10030345.

Brand, A.S., and J.R. Roesler. 2018. "Interfacial transition zone of cement composites with steel furnace slag aggregates." *Cem. Concr. Compos.* 86: 117-129. https://doi.org/10.1016/j.cemconcomp.2017.11.012.

British Standard Institution. 1975. "BS-812: Testing Aggregates."

De Domenico, D., F. Faleschini, C. Pellegrino, and G. Ricciardi. 2018. "Structural behavior of RC beams containing EAF slag as recycled aggregate: Numerical versus experimental results." *Constr. Build. Mater.* 171: 321-337. https://doi.org/10.1016/j.conbuildmat.2018.03.128.

Dong, B., X. Ma, Z. Zhang, H. Zhang, R. Chen, Y. Song, M. Shen, and R. Xiang. 2020. "Carbon emissions, the industrial structure and economic growth: Evidence from heterogeneous industries in China." *Environ. Pollut.* 262: 114322. https://doi.org/10.1016/j.envpol.2020.114322.

EC-2. 2010. "Eurocode 2: Design of concrete structures. Part 1-1: General rules and rules for buildings." CEN (European Committee for Standardization).

EN-Euronorm. Rue de stassart, 36. Belgium-1050 Brussels, European Committee for Standardization.

Fronek, B., P. Bosela, and N. Delatte. 2012. "Steel slag aggregate used in portland cement concrete." *Transp. Res. Rec.* 2267: 37-42. https://doi.org/10.3141/2267-04.

Fuente-Alonso, J.A., V. Ortega-López, M. Skaf, Á. Aragón, and J.T. San-José. 2017. "Performance of fiber-reinforced EAF slag concrete for use in pavements." *Constr. Build. Mater.* 149: 629-638. https://doi.org/10.1016/j.conbuildmat.2017.05.174.

Golestani, B., H. Maherinia, B.H. Nam, and A. Behzadan, Investigation on the effects of recycled asphalt shingle as an additive to hot-mix asphalt, in: J.T. Harvey, K.F. Chou (Eds.) 2015 International Airfield and Highway Pavements Conference: Innovative and Cost-Effective Pavements for a Sustainable Future, American Society of Civil Engineers (ASCE), 2015, pp. 9-18.

González-Ortega, M.A., S.H.P. Cavalaro, G. Rodríguez de Sensale, and A. Aguado. 2019. "Durability of concrete with electric arc furnace slag aggregate." *Constr. Build. Mater.* 217: 543-556. https://doi.org/10.1016/j.conbuildmat.2019.05.082.

Güneyisi, E., M. Gesoğlu, Z. Algin, and H. Yazici. 2014. "Effect of surface treatment methods on the properties of self-compacting concrete with recycled aggregates." *Constr. Build. Mater.* 64: 172-183. https://doi.org/10.1016/j.conbuildmat.2014.04.090.

Hák, T., S. Janoušková, B. Moldan, and A.L. Dahl. 2018. "Closing the sustainability gap: 30 years after “Our Common Future” society lacks meaningful stories and relevant indicators to make the right decisions and build public support." *Ecol. Indic.* 87: 193-195. https://doi.org/10.1016/j.ecolind.2017.12.017.

Kim, J.M., S.M. Choi, and D. Han. 2016. "Improving the mechanical properties of rapid air cooled ladle furnace slag powder by gypsum." *Constr. Build. Mater.* 127: 93-101. https://doi.org/10.1016/j.conbuildmat.2016.09.102.

Koenig, A. 2020. "Analysis of air voids in cementitious materials using micro X-ray computed tomography (µXCT)." *Constr. Build. Mater.* 244: 118313. https://doi.org/10.1016/j.conbuildmat.2020.118313.

Ladomerský, J., I. Janotka, E. Hroncová, and I. Najdená. 2016. "One-year properties of concrete with partial substitution of natural aggregate by cupola foundry slag." *J. Clean. Prod.* 131: 739-746. https://doi.org/10.1016/j.jclepro.2016.04.101.

Larsen, I.L., and R.T. Thorstensen. 2020. "The influence of steel fibres on compressive and tensile strength of ultra high performance concrete: A review." *Constr. Build. Mater.* 256: 119459. https://doi.org/10.1016/j.conbuildmat.2020.119459.

Lee, J.Y., J.S. Choi, T.F. Yuan, Y.S. Yoon, and D. Mitchell. 2019. "Comparing properties of concrete containing electric arc furnace slag and granulated blast furnace slag." *Materials* 12 (9): 1371. https://doi.org/10.3390/ma12091371.

Li, Z., K. Afshinnia, and P.R. Rangaraju. 2016. "Effect of alkali content of cement on properties of high performance cementitious mortar." *Constr. Build. Mater.* 102: 631-639. https://doi.org/10.1016/j.conbuildmat.2015.10.110.

Liew, K.M., and A. Akbar. 2020. "The recent progress of recycled steel fiber reinforced concrete." *Constr. Build. Mater.* 232: 117232. https://doi.org/10.1016/j.conbuildmat.2019.117232.

Lim, J.S., C.B. Cheah, and M.B. Ramli. 2019. "The setting behavior, mechanical properties and drying shrinkage of ternary blended concrete containing granite quarry dust and processed steel slag aggregate." *Constr. Build. Mater.* 215: 447-461. https://doi.org/10.1016/j.conbuildmat.2019.04.162.

Majhi, R.K., and A.N. Nayak. 2020. "Production of sustainable concrete utilising high-volume blast furnace slag and recycled aggregate with lime activator." *J. Clean. Prod.* 255: 120188. https://doi.org/10.1016/j.jclepro.2020.120188.

Manso, J.M., V. Ortega-López, J.A. Polanco, and J. Setién. 2013. "The use of ladle furnace slag in soil stabilization." *Constr. Build. Mater.* 40: 126-134. https://doi.org/10.1016/j.conbuildmat.2012.09.079.

Martínez-Lage, I., P. Vázquez-Burgo, and M. Velay-Lizancos. 2020. "Sustainability evaluation of concretes with mixed recycled aggregate based on holistic approach: Technical, economic and environmental analysis." *Waste Manage.* 104: 9-19. https://doi.org/10.1016/j.wasman.2019.12.044.

Mehta, A., R. Siddique, T. Ozbakkaloglu, F. Uddin Ahmed Shaikh, and R. Belarbi. 2020. "Fly ash and ground granulated blast furnace slag-based alkali-activated concrete: Mechanical, transport and microstructural properties." *Constr. Build. Mater.* 257: 119548. https://doi.org/10.1016/j.conbuildmat.2020.119548.

Montenegro-Cooper, J.M., M. Celemín-Matachana, J. Cañizal, and J.J. González. 2019. "Study of the expansive behavior of ladle furnace slag and its mixture with low quality natural soils." *Constr. Build. Mater.* 203: 201-209. https://doi.org/10.1016/j.conbuildmat.2019.01.040.

NLT-361. 1991. "Determination of the ageing degree in steel slag."

Ortega-López, V., J.A. Fuente-Alonso, A. Santamaría, J.T. San-José, and Á. Aragón. 2018. "Durability studies on fiber-reinforced EAF slag concrete for pavements." *Constr. Build. Mater.* 163: 471-481. https://doi.org/10.1016/j.conbuildmat.2017.12.121.

Ortega-López, V., A. García-Llona, V. Revilla-Cuesta, A. Santamaría, and J.T. San-José. 2021. "Fiber-reinforcement and its effects on the mechanical properties of high-workability concretes manufactured with slag as aggregate and binder." *J. Build. Eng.* 43: 102548. https://doi.org/10.1016/j.jobe.2021.102548.

Ortega-López, V., J.M. Manso, I.I. Cuesta, and J.J. González. 2014. "The long-term accelerated expansion of various ladle-furnace basic slags and their soil-stabilization applications." *Constr. Build. Mater.* 68: 455-464. https://doi.org/10.1016/j.conbuildmat.2014.07.023.

Papayianni, I., S. Konopisi, and F. Kesikidou, Physico-mechanical properties and durability aspects of alkali-activated calcareous fly ash/slag mortars, in: S. Nenadalova, V. Bilek, Z. Kersner, H. Simonova, S. Seitl, V. Bilek (Eds.) 6th International Conference Non-Traditional Cement and Concrete, 2017, Trans Tech Publications Ltd, 2018, pp. 87-91.

Park, J.J., D.Y. Yoo, S. Kim, and S.W. Kim. 2019. "Benefits of synthetic fibers on the residual mechanical performance of UHPFRC after exposure to ISO standard fire." *Cem. Concr. Compos.* 104: 103401. https://doi.org/10.1016/j.cemconcomp.2019.103401.

Parron-Rubio, M.E., F. Perez-García, A. Gonzalez-Herrera, and M.D. Rubio-Cintas. 2018. "Concrete properties comparison when substituting a 25% cement with slag from different provenances." *Materials* 11 (6): 1029. https://doi.org/10.3390/ma11061029.

Qasrawi, H. 2018. "Fresh properties of green SCC made with recycled steel slag coarse aggregate under normal and hot weather." *J. Clean. Prod.* 204: 980-991. https://doi.org/10.1016/j.jclepro.2018.09.075.

Revilla-Cuesta, V., M. Skaf, F. Faleschini, J.M. Manso, and V. Ortega-López. 2020a. "Self-compacting concrete manufactured with recycled concrete aggregate: An overview." *J. Clean. Prod.* 262: 121362. https://doi.org/10.1016/j.jclepro.2020.121362.

Revilla-Cuesta, V., M. Skaf, J.M. Manso, and V. Ortega-López. 2020b. "Student perceptions of formative assessment and cooperative work on a technical engineering course." *Sustainability* 12 (11): 4569. https://doi.org/10.3390/su12114569.

Roslan, N.H., M. Ismail, N.H.A. Khalid, and B. Muhammad. 2020. "Properties of concrete containing electric arc furnace steel slag and steel sludge." *J. Build. Eng.* 28: 101060. https://doi.org/10.1016/j.jobe.2019.101060.

Salcedo, J.C., and M. Fortea. 2020. "The influence of structural alterations on the damages of the Amatrice earthquake, Italy (2016)." *Inf. Constr.* 72 (559): 71378. https://doi.org/10.3989/IC.71378.

San-José, J.T., and J.M. Manso. 2006. "Fiber-reinforced polymer bars embedded in a resin concrete: Study of both materials and their bond behavior." *Polym. Compos.* 27 (3): 315-322. https://doi.org/10.1002/pc.20188.

Santamaria, A., F. Faleschini, G. Giacomello, K. Brunelli, J.T. San José, C. Pellegrino, and M. Pasetto. 2018. "Dimensional stability of electric arc furnace slag in civil engineering applications." *J. Clean. Prod.* 205: 599-609. https://doi.org/10.1016/j.jclepro.2018.09.122.

Santamaría, A., A. García-Llona, V. Revilla-Cuesta, I. Piñero, and V. Ortega-López. 2021. "Bending tests on building beams containing electric arc furnace slag and alternative binders and manufactured with energy-saving placement techniques." *Structures* 32: 1921-1933. https://doi.org/10.1016/j.istruc.2021.04.003.

Santamaría, A., J.J. González, M.M. Losáñez, M. Skaf, and V. Ortega-López. 2020a. "The design of self-compacting structural mortar containing steelmaking slags as aggregate." *Cem. Concr. Compos.* 111: 103627. https://doi.org/10.1016/j.cemconcomp.2020.103627.

Santamaría, A., A. Orbe, M.M. Losañez, M. Skaf, V. Ortega-Lopez, and J.J. González. 2017. "Self-compacting concrete incorporating electric arc-furnace steelmaking slag as aggregate." *Mater. Des.* 115: 179-193. https://doi.org/10.1016/j.matdes.2016.11.048.

Santamaría, A., A. Orbe, J.T. San José, and J.J. González. 2018. "A study on the durability of structural concrete incorporating electric steelmaking slags." *Constr. Build. Mater.* 161: 94-111. https://doi.org/10.1016/j.conbuildmat.2017.11.121.

Santamaría, A., V. Ortega-López, M. Skaf, J.A. Chica, and J.M. Manso. 2020b. "The study of properties and behavior of self compacting concrete containing Electric Arc Furnace Slag (EAFS) as aggregate." *Ain Shams Eng. J.* 11 (1): 231-243. https://doi.org/10.1016/j.asej.2019.10.001.

Santamaría, A., E. Rojí, M. Skaf, I. Marcos, and J.J. González. 2016. "The use of steelmaking slags and fly ash in structural mortars." *Constr. Build. Mater.* 106: 364-373. https://doi.org/10.1016/j.conbuildmat.2015.12.121.

Selleck, S.F., E.N. Landis, M.L. Peterson, S.P. Shah, and J.D. Achenbach. 1998. "Ultrasonic investigation of concrete with distributed damage." *ACI Mater. J.* 95 (1): 27-36.

Sideris, K.K., C. Tassos, A. Chatzopoulos, and P. Manita. 2018. "Mechanical characteristics and durability of self compacting concretes produced with ladle furnace slag." *Constr. Build. Mater.* 170: 660-667. https://doi.org/10.1016/j.conbuildmat.2018.03.091.

Silva, R.V., J. de Brito, and R.K. Dhir. 2019. "Use of recycled aggregates arising from construction and demolition waste in new construction applications." *J. Clean. Prod.* 236: 117629. https://doi.org/10.1016/j.jclepro.2019.117629.

Skaf, M., E. Pasquini, V. Revilla-Cuesta, and V. Ortega-López. 2019. "Performance and durability of porous asphalt mixtures manufactured exclusively with electric steel slags." *Materials* 12 (20): 3306. https://doi.org/10.3390/ma12203306.

Tanaka, K., R. Kawasaki, T. Katayama, and Y. Morita, Evaluation of mechanical properties of dimpled PET fiber fabricated by electrospinning method, in: N. Noda, G. Chang (Eds.) 3rd International Conference on Design, Materials and Manufacturing, ICDMM 2018, Trans Tech Publications Ltd, 2018, pp. 8-14.

UNE-83982. 2008. "Concrete durability. Test methods. Determination of the capillar suction in hardened concrete. Fagerlund method."

Wang, J., Z. Guo, Q. Yuan, P. Zhang, and H. Fang. 2020. "Effects of ages on the ITZ microstructure of crumb rubber concrete." *Constr. Build. Mater.* 254: 119329. https://doi.org/10.1016/j.conbuildmat.2020.119329.

Yang, L., C. Shi, and Z. Wu. 2019. "Mitigation techniques for autogenous shrinkage of ultra-high-performance concrete – A review." *Compos. Part B: Eng.* 178: 107456. https://doi.org/10.1016/j.compositesb.2019.107456.

Yildirim, I.Z., and M. Prezzi. 2020. "Subgrade stabilisation mixtures with EAF steel slag: an experimental study followed by field implementation." *Int. J. Pavement Eng.* https://doi.org/10.1080/10298436.2020.1823389.

Yousefieh, N., A. Joshaghani, E. Hajibandeh, and M. Shekarchi. 2017. "Influence of fibers on drying shrinkage in restrained concrete." *Constr. Build. Mater.* 148: 833-845. https://doi.org/10.1016/j.conbuildmat.2017.05.093.

Zanini, M.A. 2019. "Structural reliability of bridges realized with reinforced concretes containing electric arc furnace slag aggregates." *Eng. Struct.* 188: 305-319. https://doi.org/10.1016/j.engstruct.2019.02.052.

Zhan, P.M., and Z.H. He. 2019. "Application of shrinkage reducing admixture in concrete: A review." *Constr. Build. Mater.* 201: 676-690. https://doi.org/10.1016/j.conbuildmat.2018.12.209.

Zhang, P., Z. Gao, J. Wang, J. Guo, S. Hu, and Y. Ling. 2020. "Properties of fresh and hardened fly ash/slag based geopolymer concrete: A review." *J. Clean. Prod.* 270: 122389. https://doi.org/10.1016/j.jclepro.2020.122389.